# Remodeling Articular Immune Homeostasis with an Efferocytosis-inspired Nanoimitator Mitigates Rheumatoid Arthritis

**Xinyi Jiang** ( xinyijiang@sdu.edu.cn )
Shandong University https://orcid.org/0000-0003-0074-6876
**Shengchang Zhang**
Shandong University
**Qihao Chai**
Shandong Provincial Hospital Affiliated to Shandong University
**Chunwei Tang**
Shandong University
**Ziyang Li**
Shandong Provincial Hospital Affiliated to Shandong University
**Zhentao Man**
Shandong Provincial Hospital Affiliated to Shandong University
**Chen Chen**
Shandong University
**Jing Zhang**
Shandong University
**Ying Liu**
Shandong University
**Peng Sun**
Shandong University of Traditional Chinese Medicine
**Rui Zhang**
Shandong University
**Zhenmei Yang**
Shandong University
**Maosen Han**
Shandong University
**Yan Wang**
Shandong University
**Xia Wei**
Shandong Institute for Food and Drug Contro
**Jun Li**

Shandong Institute for Food and Drug Contro

**Wei Li**

Shandong Provincial Hospital Affiliated to Shandong First Medical University

**Mohnad Abdalla**

shandong university

**Gongchang Yu**

Neck-Shoulder and Lumbocrural Pain Hospital

**Bin Shi**

Neck-Shoulder and Lumbocrural Pain Hospital

---

**Article**

**Keywords:** Efferocytosis-inspired nanoimitator, Rheumatoid arthritis, Synovial 57 inflammatory macrophage, Articular immune homeostasis, Chondroprotection

**Posted Date:** January 5th, 2022

**DOI:** https://doi.org/10.21203/rs.3.rs-1159315/v1



---

# Remodeling Articular Immune Homeostasis with an Efferocytosis-inspired Nanoimitator Mitigates Rheumatoid Arthritis

Shengchang Zhang[1], Qihao Chai[2,3], Chunwei Tang[1], Ziyang Li[2,3], Zhentao Man[2,3], Chen Chen[1], Jing Zhang[1], Ying Liu[1], Peng Sun[4], Rui Zhang[1], Zhenmei Yang[1], Maosen Han[1], Yan Wang[1], Xia Wei[5], Jun Li[5], Wei Li[2,3], Mohnad Abdalla[1], Gongchang Yu[6], Bin Shi[6], Xinyi Jiang[1,7*]

[1]Key Laboratory of Chemical Biology (Ministry of Education), Department of Pharmaceutics, School of Pharmaceutical Sciences, Cheeloo College of Medicine, Shandong University, 44 Cultural West Road, Shandong Province, 250012, China

[2]Department of orthopaedic surgery, Shandong Provincial Hospital Affiliated to Shandong University, Jinan, Shandong Province 250021, China

[3]Department of orthopaedic surgery, Shandong Provincial Hospital Affiliated to Shandong First Medical University, Jinan, Shandong Province 250021, China

[4]Shandong University of Traditional Chinese Medicine, Jinan, Shandong Province, 250355, China

[5]Department of Pharmacology and Toxicology, Shandong Institute for Food and Drug Control, Shandong Province, China

[6]Neck-Shoulder and Lumbocrural Pain Hospital, Shandong First Medical University & Shandong Academy of Medical Sciences, Jinan, China

[7]NMPA Key Laboratory for Technology Research and Evaluation of Drug Products, Shandong University, 44 Cultural West Road, Shandong Province, 250012, China

[*]Corresponding author: Xinyi Jiang, Ph.D.

Phone/Fax：+86-15662758621

Email：xinyijiang@sdu.edu.cn

**Abstract**

Massive intra-articular infiltration of the pro-inflammatory macrophages is a prominent feature of rheumatoid arthritis (RA) lesions, which are thought to underlie articular immune dysfunction, severe synovitis and ultimate joint erosion. Here we report an efferocytosis-inspired nanoimitator (EINI) for in situ targeted reprogramming of the synovial inflammatory macrophages (SIMs) and thus thwarting their autoimmune attack and reinstating articular immune homeostasis, which mitigates RA. The EINI consisted of a drug-based core with an oxidative stress-responsive phosphatidylserine (PtdSer) corona and a shell of P-selectin-blocking motif, low molecular weight heparin (LMWH). When systemically administrated, the LMWH on the EINI first bound to P-selectin overexpressed on endothelium in subsynovial capillaries, which functioned as an antagonist disrupting neutrophils synovial trafficking. Due to the high dysregulation of the synovial microvasculature, the EINI subsequently enriched in joint synovium where the shell was exfoliated upon the reactive oxygen species stimulation, and PtdSer corona was then exposed. In an efferocytosis-like manner, the PtdSer-coroneted core was in turn phagocytosed by SIMs, which synergistically terminated the SIMs-initiated pathological cascades and serially reconstructed the intra-articular immune homeostasis, conferring a chondroprotection effect. These findings demonstrate that SIMs can be precisely remodeled via the efferocytosis-mimetic strategy, which holds great potential for RA treatment.

**Key words:** Efferocytosis-inspired nanoimitator; Rheumatoid arthritis; Synovial inflammatory macrophage; Articular immune homeostasis; Chondroprotection

## Introduction

Rheumatoid arthritis (RA), a widespread and devastating systemic autoimmune disease, characterized by articular immune dysfunction with serious synovitis and joint erosion that causes progressive disability[1, 2]. Over the past two decades, multiple immunosuppressants have been approved by the U.S. FDA for RA treatment[3]. Despite combining use of these immunosuppressants, about one-third of patients with RA fail to reach sustained clinical remission[4]. Moreover, the continuous use of immunosuppressive therapeutics often weakens the immune system and do increase the risk of infections[5]. The pathogenesis of RA involves the complicated inflammatory networks, including the multiplicity of cytokine targets and a complex crosstalk of inflammatory cells[6, 7]. Among these, synovial inflammatory macrophages (SIMs) play a pivotal role in orchestrating the cytokine environment, which are thought to underlie articular immune dysfunction, synovitis and ultimate joint erosion[8, 9]. As such, terminating the SIMs-initiated cascades and serially reinstating articular immune homeostasis may be a reversible approach for RA therapy, which remains largely unexplored.

Patients with RA can be divided into two major subsets based on the presence versus absence of anti-citrullinated protein antibodies (ACPAs)[10]. The $ACPA^+$ subset of disease constitutes approximately two-thirds of all cases of RA and generally has a more severe disease course[11]. Interferon regulatory factor 5 (IRF5) is a master regulator in defining the classical inflammatory phenotype of macrophages[12] and translates various signals related to the SIMs in RA synovium[13, 14]. In humans, polymorphisms in the IRF5 genes have been associated with an increased risk of developing autoimmune disease including RA[15, 16]. Bioinformatically, we found that the expression of IRF5 revealed a positive correlation with the ACPAs titer in RA synovium (Fig. 1a). Consistently, in patients with $ACPA^+$ RA, the expression level of IRF5 protein was obviously elevated (Fig. 1b). Targeted silencing of IRF5 in SIMs may therefore be an efficient strategy that could facilitate the anti-inflammation polarization of macrophages and thus abort the SIMs-initiated cascades in $ACPA^+$ RA.

Precisely targeting intra-articular macrophages is of utmost importance for efficiently regulating SIMs-initiated cascades. The phagocytosis of the apoptotic cells, called efferocytosis, is one of the critical innate functions of macrophages, which maintains tissue homeostasis[17, 18]. During efferocytosis, phosphatidylserine (PtdSer) exposure on the outer leaflet of the plasma membrane in the apoptotic cells is a key "eat-me" signal for macrophages[19]. PtdSer coronation may therefore enhance the targeted-internalization of nano-formulation by macrophages. However, after systemic administration, PtdSer-coroneted nano-formulation may be up-taken by the pan-macrophages, which results in severe adverse effects. Of note, intra-articular oxidative stress caused by high level of reactive oxygen species (ROS) is one of the typical characteristics of RA lesions[20, 21]. As such, ROS-responsive exfoliation may be an efficient way to manipulate the locoregional exposure of PtdSer corona of the designed nano-formulation intra-articular, which enabled the specific-phagocytosis of the nano-formulation by SIMs.

Here, we sought to develop an efferocytosis-mimetic self-deliverable nanoimitator for in situ targeted reprogramming of the SIMs and thus thwarting their autoimmune attack and reinstating articular immune homeostasis for RA-reversible treatment (Fig. 1c). The siIRF5-carrying efferocytosis-inspired nanoimitator (siIRF5@EINI) was for the first time sequentially assembled by a drug-based core with an oxidative stress-responsive phosphatidylserine (PtdSer) corona and an outer shell of low molecular weight heparin (LMWH). With the shielding of LMWH, the siIRF5@EINI was endowed with the stealth property in circulation, an enhanced inflamed regions retention, and a blocking function of P-selectin that retards the articular trafficking of neutrophils (NEs). When systemically administrated, the LMWH on the nanoimitator first bound to P-selectin overexpressed on endothelium in subsynovial capillaries, which functioned as an antagonist disrupting NEs synovial trafficking. Due to the leakage of the intra-articular blood vessel, the siIRF5@EINI subsequently enriched in joint synovium where the shell was exfoliated upon the ROS stimulation, and PtdSer corona was then exposed. In an efferocytosis-like manner, the PtdSer-coroneted core

was in turn phagocyted by SIMs. We demonstrated that the siIRF5@EINI synergistically terminated the SIMs-initiated pathological cascades and reconstructed the intra-articular immune homeostasis, and ultimately conferred a chondroprotection effect and restored the joint function, all of which were comprehensively investigated with in a RA murine model.

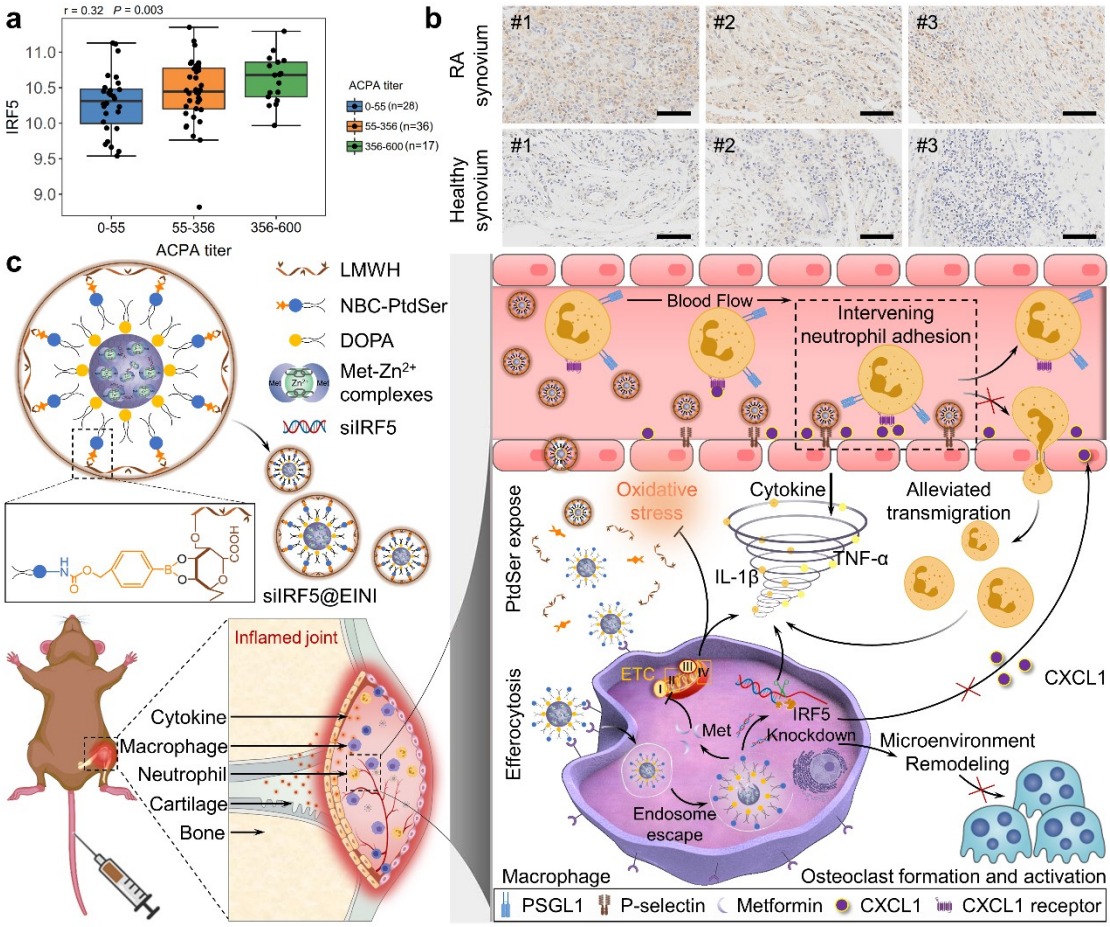


**Fig. 1 Efferocytosis-inspired nanoimitator in situ targeted silencing of IRF5 in SIMs for precision RA therapy. a** The positive correlation between the IRF5 gene expression levels and the anti-citrullinated protein antibodies (ACPAs) titer in the RA synovium (r = 0.32, $P = 0.003$). **b** Immunohistochemistry staining of IRF5 in synovium from RA patients and healthy donors (3 cases each group). Scale bar = 50 μm. **c** Schematic illustration shows that the efferocytosis-inspired nanoimitator terminates the SIMs-initiated pathological cascades, synergistically restores the articular immune homeostasis, and ultimately reverses bone erosion.

## Results

### Preparation and characterization of EINI

Via conjugating 4-nitrophenyl 4-(4,4,5,5-tetramethyl-1,3,2-dioxaborolan-2-yl) benzyl carbonate (NBC) with PtdSer, we first synthesized a ROS-responsive PtdSer-NBC conjugate (Supplementary Fig. 1, 2). The efferocytosis-inspired nanoimitator was prepared (Fig. 2a). Briefly, dioleoylphosphatydic acid (DOPA) stabilized siIRF5-laden metformin-$Zn^{2+}$-based nanocore was constructed using the reverse microemulsion method, and then coroneted with PtdSer-NBC. Subsequently, the corona of nanocore was cloaked with LWMH via a reversible boronate ester linker by the reaction of cis-diols and phenylboronic acid groups, and the siIRF5-laden efferocytosis-inspired nanoimitator (siIRF5@EINI) was thus achieved. Under transmission electron microscopy (TEM) (Fig. 2b), the obtained nanoimitator showed a spherical morphology with a hydrodynamic diameter of ~72 nm (Fig. 2c). After dual coating with PtdSer-NBC and LWMH, the zeta potential of the nano-formulation decreased from 44.5 ± 0.4 mV to -18.7 ± 0.03 mV (Fig. 2c and Supplementary Fig. 3). We next investigated the stimulation-triggered presenting of PtdSer of the siIRF5@EINI in an RA-mimicking microenvironment. As shown in Fig. 2d and Supplementary Fig. 4, 72.61% of the PtdSer-presenting nanoparticles were determined to band to fluorescein isothiocyanate (FITC)-annexin V in the solution of 0.1 mM $H_2O_2$, which was merely 18.23% in PBS control group, indicating oxidative stress in RA tissues could convert PtdSer-NBC of the nanoimitator into PtdSer.

Next, we evaluated the acid-triggered drug release of the nanoimitator in vitro. The morphology of nanoimitator exhibited significant degradation into ultrasmall species in acidic environments as shown by the TEM images (Fig. 2e). Structural disassembly was further confirmed with dynamic light scattering (DLS) assay as shown in the embedded image of Fig. 2e. Consistently, we found that under acidic conditions (pH 5.0), the release of metformin from the nanoimitator increased compared to that under physiological conditions (pH 7.4) (Fig. 2f). With electrophoresis assay (Fig. 2h), siIRF5 release profile was also monitored. At lysosomal pH of 5.0, siIRF5 burst released from

the nano-formulation, while at physical pH of 7.4, we did not detect any release of siIRF5 from the siIRF5@EINI. The ROS-responsive exfoliation of the EINI was further determined with the $H_2O_2$ scavenging assay. Fig. 2g revealed a time-dependent ROS elimination of the nanoimitator upon the ROS stimulation, implying the ROS-stimulated deshielding of the nanoimitator in the RA pathological condition.

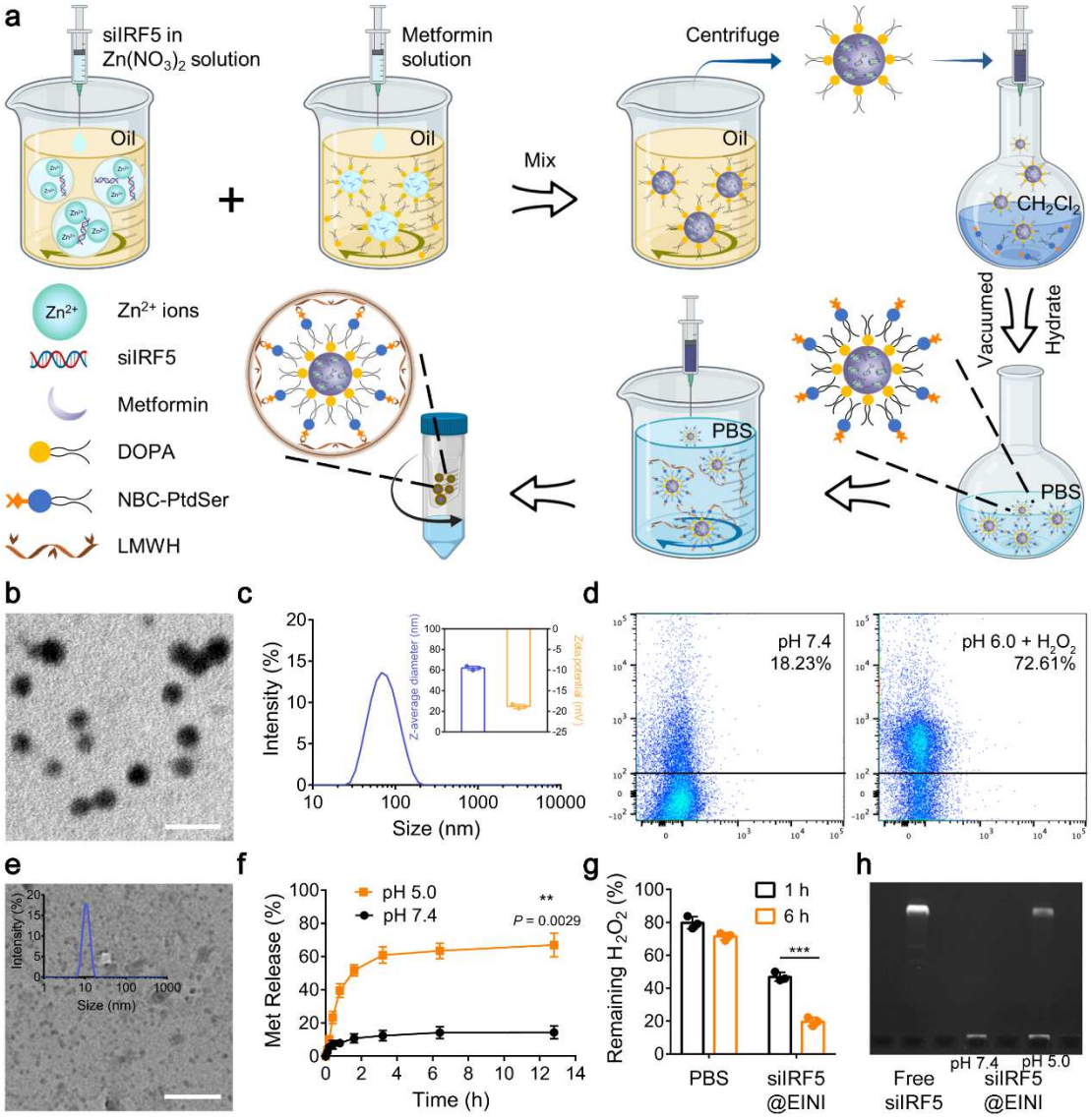


**Fig. 2 Preparation and characterization of siIRF5@EINI. a** Schematic of the preparation of nanoimitator by a modified reverse microemulsion method. **b** Transmission electron microscope image of siIRF5@EINI. Scale bar = 100 nm. **c** Hydrodynamic size and zeta potential determined with DLS. Data are presented as the mean ± s.d. ($n$ = 3 independent experiments). **d** Flow cytometry analysis of PtdSer-presenting. ($n$ = 3 independent experiments). **e** TEM images of the nanoimitator after

triggered degradation under acidic conditions (pH 5.0). Scale bar = 100 nm. **f** Drug release of the nanoimitator in PBS at different pH values. Data are presented as the mean ± s.d. ($n$ = 3 independent experiments). $^{**}P < 0.01$. **g** ROS scavenging ability of nanoimitator. Results are reported as the mean ± s.d. ($n$ = 3 independent experiments). $P$ value was calculated by comparing with group PBS. $^{***}P < 0.001$. **h** Electrophoretic gel assay showing the pH-responsive release of siIRF5 from the nanoimitator. The experiments were repeated three times, independently.

**Cellular engulfment specificity of the nanoimitator in vitro**

PtdSer exposure triggers the efferocytosis of macrophages (Fig. 3a). We next determined the engulfment and intracellular trafficking of the nano-formulation in vitro using bone marrow derived macrophages (BMDMs) that were isolated from mouse (Supplementary Fig. 5). BMDMs were pre-activated with TNF-α and then treated with the nanoimitator that was pre-conditioned with the 0.1mM $H_2O_2$. As shown in Fig. 3b, significant fluorescence was detected in BMDMs, indicating that abundant nanoimitators were engulfed into BMDMs. With fibroblast-like synoviocytes (FLSs) as a control, we also determined the cellular engulfment specificity of the nanoimitator. Minimal Cy5.5 signal was detected in FLSs (Fig. 3b). The results indicate that the EINI was specifically engulfed by macrophages when ROS existed. Moreover, under an RA-mimetic condition, an increased fluorescent intensity was determined in macrophages compared to that under physiological microenvironment. A similar trend was found in flow cytometry quantification (Fig. 3c). With a co-culture system, we further compared the uptake of the nanoimitator by the pre-activated macrophages or FLSs under an RA-mimetic condition. Consistently, fluorescence visualization with confocal laser scanning microscope (CLSM) also indicates the specific engulfment of the PtdSer-coroneted core by macrophages rather than FLSs (Fig. 3d). Next, we wished to ascertain whether the siIRF5-laden nanoimitator would escape lyso/endosome and release the payloads in cytoplasm after efficient up-taken by the macrophages. Co-localization with CLSM revealed the nanoimitators were internalized by the cell via an endocytosis pathway and then escaped from lyso/endosome, during which the payloads were

released into cytoplasm (Fig. 3e, f and Supplementary Fig. 6). Collectively, these results indicated that ROS-responsive exposure of PtdSer in the siIRF5@EINI induced an efficient phagocytosis by macrophages, and the lysosomal pH-triggered dissociation of the nanocarrier resulted in a successful lyso/endosome escape.

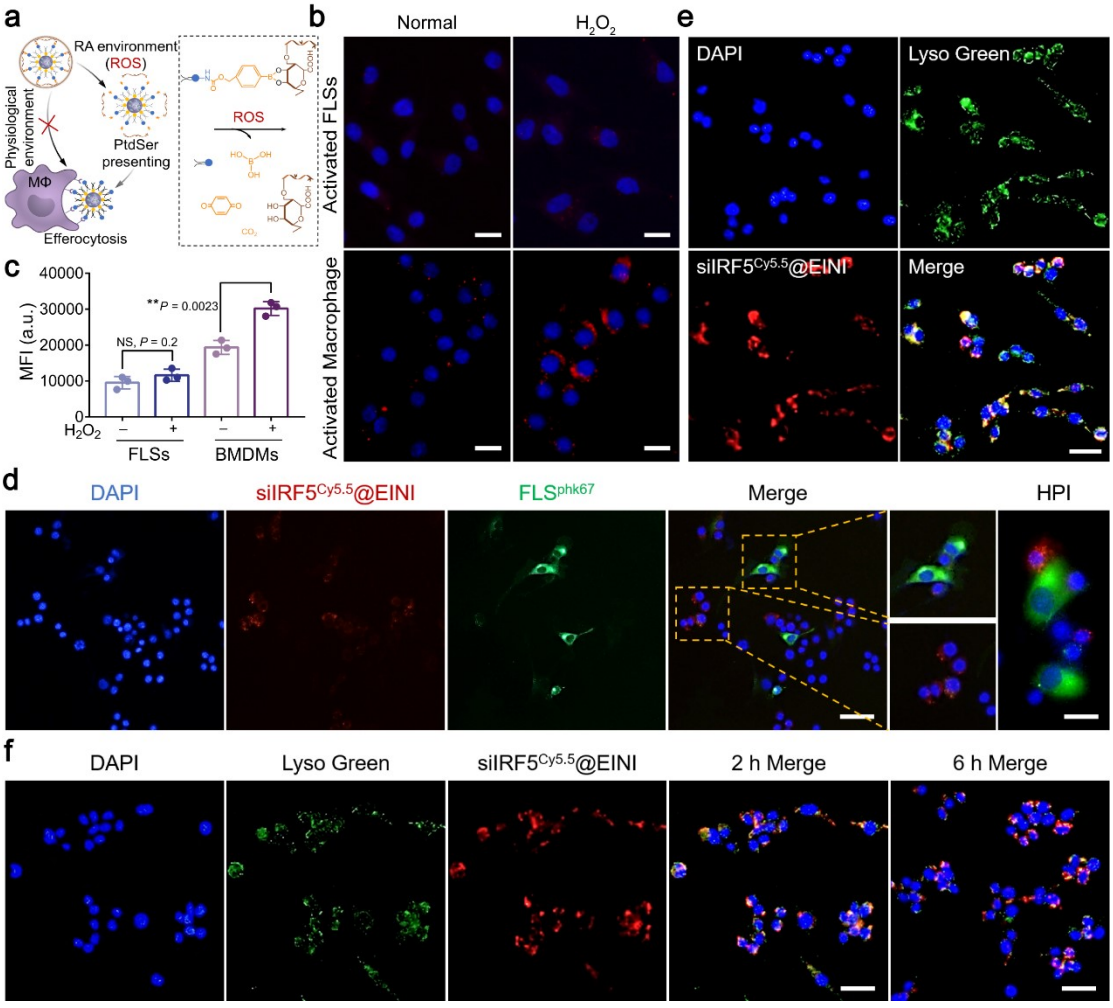


**Fig. 3 Cellular uptake and intracellular distribution of the nano-formulation. a** Mechanistic explanation for the specific engulfment of the nanoimitator by macrophages. **b** Fluorescent images of macrophages and FLSs after incubation with siIRF5@EINI that with or without $H_2O_2$ pre-treating. Cells were activated with TNF-α before nano-formulation incubation. Scale bar, 20 μm. **c** Flow cytometric analysis of nanoparticle binding to macrophages or FLSs. Data are presented as the mean ± s.d. ($n$ = 3 independent experiments). $^{**}P < 0.01$. NS, not significant. **d** Representative images of $H_2O_2$-pretreated siIRF5@EINI (red) engulfed by macrophages (not labeled)/FLSs (green) in a co-culture pattern. Scale bar, 50 nm. The right panel shows the

representative high power images (HPI). Scale bar, 20 μm. **e** Observation of engulfment pathway of the nanoimitator. Scale bars, 20 μm. **f** Fluorescent visualization of siRNA localization in macrophages 1 or 6 hours after incubation with siIRF5@EINI. Scale bar, 50 μm. In all datasets, the experiments were repeated three times, independently.

**Inflammatory modulation of the nano-formulation**

Comprehensively regulating the production of pro-inflammatory cytokines, oxidative stress, and recruitment of NEs is essential for reestablishing articular immune homeostasis (Fig. 4a). LMWH can block P-selectin initiated cell adhesion cascade, and thus inhibit NEs migration into the inflamed regions[22]. We next evaluated the intervene effect of the nanoimitator with a monolayer model of TNF-α activated human umbilical vein endothelial cells (HUVECs). The results showed that the adhesion of NEs to HUVECs significantly decreased after pre-incubation with the nanoimitator, comparable to that treated with P-selectin antagonist (Fig. 4b and Supplementary Fig. 8). We further examined the gene silencing efficiency of the nano-formation after up-taken by macrophages. As shown in Fig. 4c, the relative level of IRF5 mRNA from TNF-α activated BMDMs revealed a dramatically decrease after treatment with the siIRF5@EINI, which is well consistent with the protein data determined by western blot (Supplementary Fig. 9). IRF5 plays a critical role in the secretion of multiple chemokines including macrophage-derived chemokine CXCL1, a neutrophil attractant[14]. We also detected the secreting level of CXCL1 from the treated macrophages. As shown in Fig. 4d, treatment with siIRF5@EINI dramatically downregulated macrophage-derived CXCL1 expression (Fig. 4d). Furthermore, neutrophil migration was also examined. We found that IRF5 ablation significantly inhibited the transendothelial migration of NEs (Fig. 4e). Therefore, we inferred that the nanoimitator may function as an antagonist disrupting the synovial trafficking of neutrophils.

Macrophages are phenotypically plastic[23]. The expression of IRF5 in macrophages defines the classical inflammatory phenotype[12]. We next evaluated the modulative effect of the nano-formulations on the phenotype conversion of the macrophages. As

shown in Fig. 4f, treatment of the siIRF5@EINI reduced the mRNA expression level of pro-inflammatory markers including tumor necrosis factor-α (TNF-α) and inducible nitric oxide synthase (iNOS), meanwhile significantly increased the levels of anti-inflammatory markers like mannose receptor (CD206) and arginase-1 (Arg-1). Similar results were obtained in the immunofluorescence-stained images of BMDMs (Fig. 4g, h). Notably, treatment with metformin-single laden nano-formulation demonstrated a strong elevation of M2-like subpopulation with highly expressed CD206. Concurrent RNAi-mediated gene silencing and metformin-mediated metabolism reprogramming further increased the immunoregulatory phenotype conversion of macrophages. Metformin can target the transport chain of mitochondrial electron and thus reprogram mitochondrial metabolism[24, 25]. As shown in Supplementary Fig. 10a, b, metformin-related treatment significantly prevented the over-zealous ROS, which synergistically leads to immunoregulatory phenotype conversion. ROS generating efficiency was also evaluated by the determination of the ratio of $NAD^+$/NADH. As shown in Supplementary Fig. 10c, a significant reduction of the ratio of $NAD^+$/NADH was detected in macrophages treated with metformin-related formulation. These results suggested the siIRF5@EINI could boost the re-programming of macrophages to an immunoregulatory phenotypes and thus significantly reduce macrophage-derived pro-inflammatory cytokines, which is conducive to reestablishing the articular immune homeostasis.

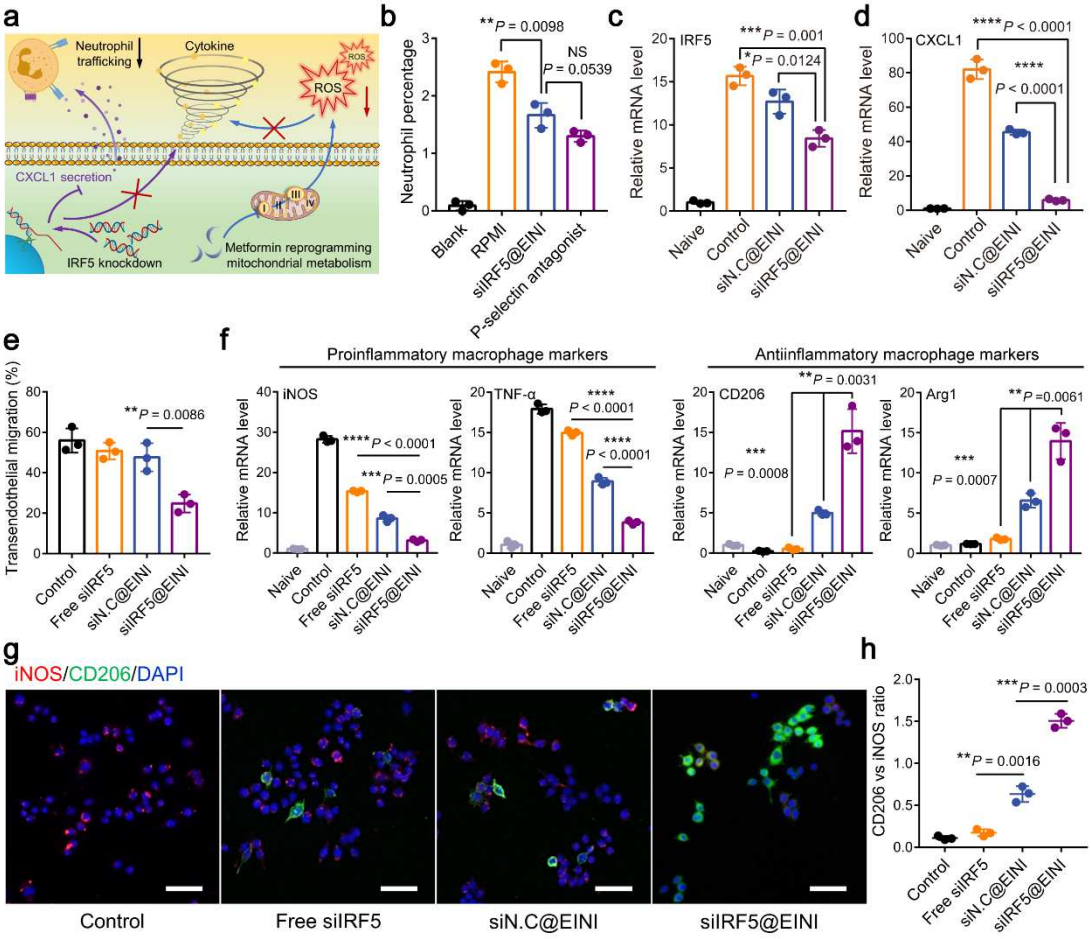


**Fig. 4 Inflammatory modulation of the nanoimitator**. **a** Schematic illustration of siIRF5@EINI-induced inflammatory regulation. **b** Quantitative analysis of the adhered neutrophils on HUVECs monolayers. The culture medium RPMI was used as a negative control. Data are presented as the mean ± s.d. ($n$ = 3 independent experiments). $^{**}P <$ 0.01. NS, not significant. **c**, **d** IRF5 (**c**) and CXCL1 (**d**) mRNA expression level in activated macrophages treated with each formulation. Data are shown as the mean ± s.d. ($n$ = 3 independent experiments). $^{*}P < 0.05$, $^{***}P < 0.001$, $^{****}P < 0.0001$. **e** The ratio of transendothelial neutrophils compared with all neutrophils after intervention with different treatments on the HUVECs monolayer model. The monolayers of HUVECs were stimulated with 10 ng/ml TNF-α. Data are shown as the mean ± SD ($n$ = 3 independent experiments). $^{**}P < 0.01$. NS, not significant. **f** qRT-PCR analysis of the phenotypical changes of the macrophages that were pre-treated with the nanoimitator in vitro. Data are presented as the mean ± s.d. ($n$ = 3 independent experiments). $^{**}P < 0.01$, $^{***}P < 0.001$, $^{****}P < 0.0001$. **g**, **h** Immunostaining of the

macrophages with different phenotypes (**g**) and the corresponding quantification of the relative fluorescence intensity (**h**). Cells were pre-treated with TNF-α and then incubated with each formulation for 24 h. Data are presented as the mean ± s.d. ($n = 3$ independent experiments). $^{**}P < 0.01$, $^{***}P < 0.001$. Scale bars, 50 nm.

**Articular localization of the nano-formulation in vivo**

A collagen-induced arthritis (CIA) murine model was first established as previously reported[26, 27]. In vivo biodistribution and pharmacokinetic properties of the self-deliverable nanoimitator were next evaluated. As shown in Fig. 5a, the EINI efficiently deposited in the inflamed joints of the diseased mice 48 h post intravenous administration. The major organs and paws of the mice from each group were collected 48 hours post-injection and subjected to fluorescence analysis ex vivo. The EINI showed prominently enriched in the arthritic area of the CIA mice (Fig. 5b). Quantification of the fluorescent intensity further confirmed that a significant increase in mean fluorescence intensity (MFI) in EINI-treated mice than that in the free drug-treated group (Fig. 5c). The articular-targeted accumulation of the nano-formulation was also imaged using a hybrid microcomputed tomography-fluorescence tomography (μCT-FLT) device. As depicted in Fig. 5d, the EINI achieved an increased accumulation in the inflamed joints. The retention profile of the nanoimitator in the synovium of arthritic joints was further evaluated. 72 h after each treatment, the CIA mice were sacrificed and the synovium cryosections were conducted. Fig. 5e, f revealed the EINI preferentially enriched in the inflammatory synovial sites compared to that from free dye-treated group. Further immunofluorescent staining demonstrated Cy5.5-labeled siIRF5 co-localized with the synovial macrophages (Fig. 5g), indicating that the EINI could efficiently accumulate intra-articular and specifically target synovial macrophages in situ.

The potential toxicity of the systemic administrated nano-formulation was also tested. No adverse effect was detected in hematological assay of the treated mice in terms of white blood cell (WBC) and red blood cell (RBC) count and the hemoglobin (HGB) (Supplementary Fig. 11a). Splenocytes were also isolated and evaluated. As

shown in Supplementary Fig. 11b, no obvious apoptosis was detected in the treated mice. Histological analysis of organs coincidentally revealed the biosafety of the nanoimitator in vivo (Supplementary Fig. 11c).

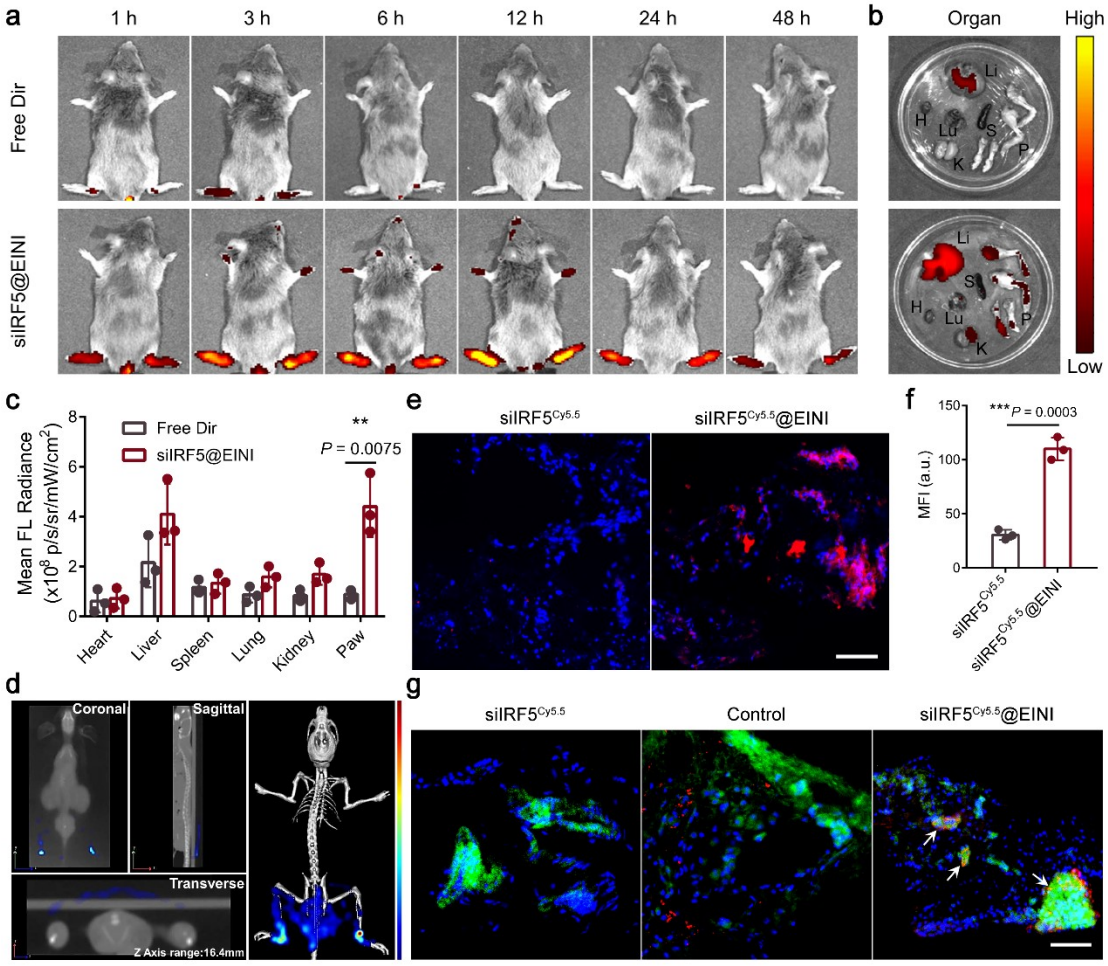


**Fig. 5 EINI selectively enriched in the inflamed joints of the CIA mice. a** In vivo fluorescence images of CIA models taken at different time points post injected with Dir labeled EINI and free Dir, respectively. **b** The fluorescence images of the excised major organs and paws harvested from the mice at 48 h post injection. **c** Quantification of fluorescence intensity in the inflamed joints and major organs of the CIA mice. Data are the mean ± s.d. ($n$ = 3 independent experiments). $^{**}P < 0.01$. **d** μCT-FLT imaging at 48 h after intravenous administration with the nanoimitators ($n$ = 3 independent experiments). **e** Trafficking profile of nanoimitator in the joint synovium. Red represents nanoimitator and blue represents nuclei. Scale bars, 50 μm. **f** Quantitative analysis of the accumulation of the nano-formulation in the synovium of the treated

mice. Data are presented as the mean ± s.d. ($n$ = 3 independent experiments). ***$P$ < 0.001. **g** Representative images of the nanoimitator taken up by synovial macrophages in vivo. Blue, DAPI-stained cell nuclei; Red, siIRF5$^{Cy5.5}$; Green, FITC conjugated anti-F4/80 antibodies labeled macrophages. Arrow indicates the co-localization of the nanoimitator and the SIMs labelled with anti-F4/80 antibodies. ($n$ = 3 independent experiments). Scale bars, 50 μm.

**EINI-enabled reestablishment of immune homeostasis and chondroprotection in vivo**

We next investigated the therapeutic potent of the nano-formulations using the abovementioned CIA mouse model (Fig. 6a). At the study endpoint, the transverse ankle diameter of mice injected with siIRF5@EINI significantly smaller than the PBS group, indicating a reduction inflammation and oedema formation (Fig. 6b and Supplementary Fig. 12). We subsequently performed the gait analysis of the treated mice using a catwalk system. As shown in Supplementary Fig. 13, siIRF5@EINI treatment markedly ameliorates the abnormality of the footprint patterns of the CIA mice compared with that of control groups. IRF5 gene silencing efficiency was also confirmed in vivo with the CIA mice. Treatment with siIRF5-laden nano-formulation significantly downregulated its expression in macrophages that were isolated from the arthritic joint (Fig. 6C and Supplementary Fig. 14). Consistently with the in vitro results, IRF5 silencing reduced the secretion of macrophage-derived CXCL1 in the inflamed joint (Fig. 6d), which in turn decreased the recruitment of NEs. We further detected the infiltration of NEs in inflamed joint by immunohistochemical staining with anti-myeloperoxidase (MPO). As shown in Fig. 6e and Fig. 6i, the siIRF5@EINI-treated group showed minimal MPO expression with few positively stained cells in the inflamed sites, while overwhelming MPO-positive cells were detected in the control joints. Competitively binding P-selectin on vascular endothelial cells can decrease the infiltration of NEs into arthritic joints, and thus promotes the restoration of the articular immune microenvironment[22, 28]. More importantly, treatment with the siIRF5@EINI synergistically induced phenotypic alteration of synovial macrophages (Fig. 6f and Fig.

6j) and subsequently decreased the unchecked infiltration of NEs in the RA joints which was conducive to reconstruct the articular immune homeostasis.

We next wished to ascertain whether systemic injection of the efferocytosis-inspired nanoimitator would control synovitis and reverse bone erosion in CIA mouse model. In hematoxylin and eosin (H&E)-stained sections, an almost completely recovered articular cavity with a clear interface without obvious synovitis and articular cartilage degeneration was detected in the siIRF5@EINI-treated mice (Fig. 6g and Fig. 6k), while severe pathologic changes including extensive inflammatory cell infiltration, synovial hyperplasia, pannus formation, and cartilage erosion were observed in the control group. Pannus formation in the synovial intimal lining features the pathological changes of RA[29]. Synovitis creates an oxidative stress microenvironment that actively induces a tumor-like invasive pannus and further exacerbates joint damage[20]. As shown in Supplementary Fig. 15a, the angiogenesis and leukocyte extravasation in the synovial sublining was significantly reduced in the siIRF5@EINI-treated groups compared with the others. These pathogenetic changes in the synovium implied the reversion of pannus progression. Additionally, safranin O staining showed optimal preservation of cartilage structure of the mice in the siIRF5@EINI-treated group (Fig. 6h and Fig. 6l). Consistent with the therapeutic efficacy results, tartrate-resistant acid phosphatase (TRAP) staining of osteoclasts further demonstrated that siIRF5@EINI treatment significantly decreased the number of osteoclasts in RA joints and achieved the slightest bone erosion (Supplementary Fig. 15b). CT was also performed to assess bone erosion. As shown in Fig. 6m, the reconstructed micro-CT images revealed that both of the ankle and the toe joints of the mice in the control groups suffered the most serious bone corrosion. Quantitative analyses of bone mineral density (BMD) demonstrated that the mean BMD in siIRF5@EINI-treated mice was almost completely recovered comparable with the healthy mice (Fig. 6n). To evaluate the potential systemic immune response, we further examined the serum levels of TNF-α and IL-1β in CIA mice. As summarized in Fig. 6o, these inflammation-related cytokines decreased after treatment, indicating effective reduction of inflammation at the systemic level.

These results collectively suggested that the efferocytosis-inspired nanoimitator could effectively repolarize SIMs to an immunoregulatory phenotype in situ, serially reinstate the articular immune homeostasis and ultimately terminated the bone erosion.

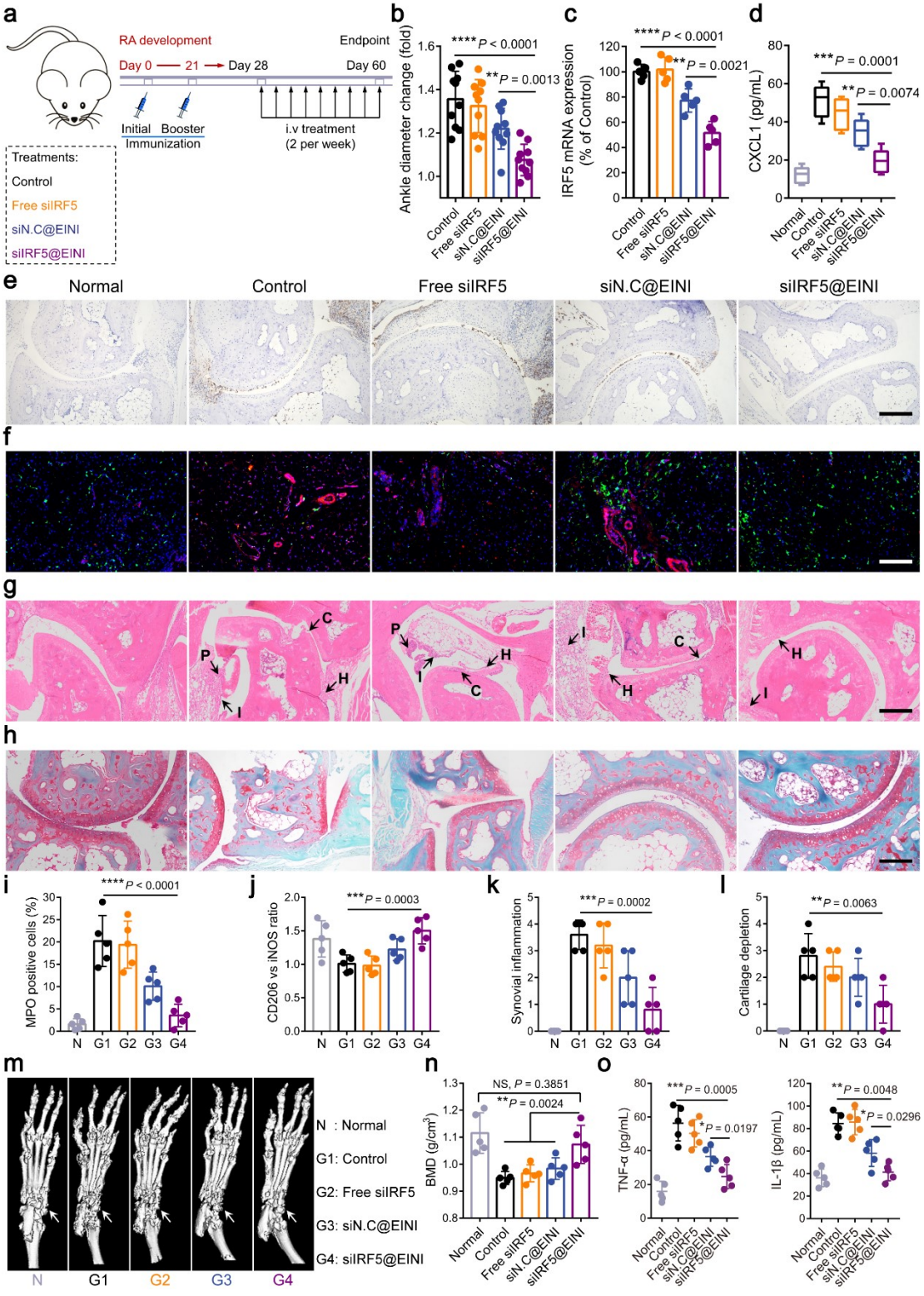


**Fig. 6 EINI-enabled reestablishment of immune homeostasis and**

**chondroprotection in vivo. a** The therapeutic regimen with a CIA mouse model. **b** Changes of the hind ankle in diameter on day 60 after CIA induction compared to that on day 0. Data are presented as the mean ± s.d. ($n$ = 5 biologically independent animals). $^{**}P < 0.01$, $^{****}P < 0.0001$. **c** Quantification of IRF5 expression in synovial macrophages after each treatment. Data are presented as the mean ± s.d. ($n$ = 5 biologically independent animals). $^{**}P < 0.01$, $^{****}P < 0.0001$. **d** Secreting level of CXCL1 in synovial tissue isolated from inflamed joint of the treated mice. Data are presented as the mean ± s.d. ($n$ = 5 biologically independent animals). $^{**}P < 0.01$, $^{***}P < 0.001$. **e** The infiltration of the neutrophils in arthritic joints in each group. Joint sections in each group were stained with anti-myeloperoxidase (MPO) antibodies. Scale bar 200 μm. ($n$ = 5 biologically independent animals). **f** Immunostaining of iNOS and CD206 (red: iNOS; green: CD206; blue: DAPI; scale bar: 50 μm) to determine the phenotype of SIMs in the CIA models treated with different formulations. ($n$ = 5 biologically independent animals). **g**, **h** Histological analysis with H&E (scale bar 200 μm) (**g**) and safranin O staining (scale bar 100 μm) (**h**) of the joint tissues that excised from the mice after different treatments. ($n$ = 5 biologically independent animals). H, synovium hyperplasia; I, immune cell infiltration; P, pannus formation; C, cartilage damage. **i-l**, The percentage of MPO-positive cells in panel e (**i**) and the ratio of the fluorescence intensity of CD206 versus iNOS in panel f (**j**). The histopathological evaluation of synovial inflammation (**k**) and cartilage depletion (**l**) were obtained from the images in (g) and (h), respectively. Data are presented as the mean ± s.d. ($n$ = 5 biologically independent animals). $^{**}P < 0.01$, $^{***}P < 0.001$, $^{****}P < 0.0001$. **m** Representative micro-CT images used for quantification of bone erosion of mice. **n** Quantification of bone mineral density determined by micro-CT. Data are presented as the mean ± s.d. ($n$ = 5 biologically independent animals). $^{**}P < 0.01$. NS, not significant. **o** Concentration profiles of TNF-α and IL-1β in serum of CIA mice treated with different groups. Data are presented as the mean ± s.d. ($n$ = 5 biologically independent animals). $^{*}P < 0.05$, $^{**}P < 0.01$, $^{***}P < 0.001$. NS, not significant.

## Discussion

The current standard-of-care therapies in clinic for patients with rheumatoid arthritis (RA) are palliative, which are still largely relying on multiple immunosuppressants[3]. Despite trying multiple different immunosuppressants, about one-third of RA patients fail to achieve disease remission[4]. Most available immunosuppressants therapies suppress the immune system systemically, which increase the risk of infections[5]. Although the precise mechanism of RA remains elusive, the latest clinical pathogenic insights indicate that extensive infiltration of inflammatory cells occurred during RA formation and aggravation[30]. Of these cells, synovial inflammatory macrophages (SIMs) are key players that involved in various proinflammatory cytokine secretion, leading to the unchecked neutrophil transmigration and initialing osteoclast-dependent cartilage destruction and bone erosion[8, 9, 31]. To precisely reprogram SIMs for RA treatment, we developed the efferocytosis-inspired nanoimitator (EINI) for terminating the SIMs-initiated pathological cascades, which could serially reconstruct the intra-articular immune homeostasis, conferring a chondroprotection effect, and ultimately restore the joint function.

RA is a systemic autoimmune disease[1]. Symmetrical inflammatory polyarthritis is the primary clinical manifestation, usually beginning in the small joints of the hands and the feet, spreading later to the larger joints[32]. Tracking and targeting inflamed joint synovium is of utmost importance for the treatment of this systemic autoimmune disease. Efferocytosis is one of the critical innate functions of macrophages, which maintains tissue homeostasis[17, 18]. PtdSer exposure on the outer leaflet of the plasma membrane in the apoptotic cells is a key "eat-me" signal for macrophages[19]. The recognition of PtdSer by macrophages mainly depends on its head group[33]. We demonstrated that PtdSer-coroneted core displayed a boosted internalization by macrophages both in vitro (Fig. 3b) and in vivo (Fig. 5g). Surficial painting of LMWH on the PtdSer-coroneted core subdued the innate vulnerability of PtdSer to phagocytosis of the mononuclear phagocyte system in blood stream, thus avoiding rapid clearance

(Fig. 5a). Moreover, the LMWH motif endowed the EINI with an enhanced retention in the inflamed regions (Fig. 5b and Fig. 5c) and a competitively inhibiting function towards P-selectin[22] that disrupts the unchecked articular trafficking of NEs (Fig. 6e). Due to the leakage of the intra-articular blood vessel, the EINI subsequently enriched in joint synovium where the shell was exfoliated upon the ROS stimulation, and PtdSer corona was then exposed. In an efferocytosis-like manner, the PtdSer-coroneted core was in turn phagocytosed by SIMs (Fig. 5g).

Polymorphisms in IRF5 genes are associated with an increased risk of developing RA (Fig. 1a, b)[15]. IRF5 translates various signals related to the pro-inflammatory macrophages in joint synovium, including the secretion of neutrophil attractants-chemokine CXCL1[14]. IRF5 deficiency supported a reduction in macrophage-derived CXCL1 and limits neutrophil infiltration into the inflamed joint. Our results demonstrated that IRF5 targeted-silencing with our EINI could repolarize SIMs to anti-inflammatory phenotype (Fig. 4g and Fig. 6f), and terminated the SIMs-initiated pathological cascades, thus inhibiting the unchecked recruitment of NEs (Fig. 4e and Fig. 6e) and the initiation of the osteoclast-dependent cartilage destruction and bone erosion (Fig. 6h, n and Supplementary Fig. 15b). In addition, the metformin in the nanoimitator can prevent complex I-derived ROS and thus promote the SIMs-targeted reprogramming[24, 34]. Our data indicates the dissociated metformin from the EINI significantly decreased the production of ROS in SIMs (Supplementary Fig. 10), which further blocked the ROS-mediated inflammatory signal and was conducive to reconstructing the intra-articular immune homeostasis synergistically.

In sum, our findings establish that synovial inflammatory macrophages (SIMs) can be targeted reprogrammed for RA reversible treatment with the proposed efferocytosis-inspired nanoimitator (EINI). By manipulation of the shielding and the exposure of PtdSer on the nano-formulation, we demonstrated the SIMs in RA joints could be precisely targeted in situ. Functionally, the EINI effectively repolarized SIMs to an immunoregulatory phenotype in situ, serially terminating the SIMs-initiated pathological cascades and ultimately reinstated the articular immune homeostasis. Our

work therefore provides a regulating strategy of macrophage heterogeneity for RA reversible treatment, which may be extended to various macrophage-involving autoimmune diseases, such as atherosclerosis, idiopathic pulmonary fibrosis and inflammatory bowel disease.

## Materials and Methods

### Materials

Dioleoylphosphatydicacid (DOPA) and dioleoyl phosphatidylserine (PtdSer) were purchased from A.V.T. (Shanghai) Pharmaceutical Co.,Ltd. (Shanghai, China). Metformin, cyclohexane, Igepal CO-520 and zinc nitrate hexahydrate ($Zn(NO_3)_2 \cdot 6(H_2O)$) were obtained from Sigma-Aldrich (St. Louis, MO, USA). Low molecular weight heparin (LMWH, MW 3800~5000, Mw/Mn (PDI) = 1.34) was purchased from Melonepharma (Dalian, China). Recombinant murine macrophage colony stimulating factor (M-CSF) (315-02) and recombinant human TNF-α (300-01A) were purchased from PeproTech (Rocky Hill, USA). RPMI 1640 medium, Dulbecco's modified Eagle medium (DMEM), modified Eagle medium, trypsin EDTA, type I collagenase, fetal bovine serum (FBS), and PBS were obtained from Gibco (USA). DiR (D12731) and PKH67 were purchased from Invitrogen (USA). The anti-CD206 antibody, anti-iNOS antibody, anti-Ly-6G antibody and anti-myeloperoxidase (MPO) antibody were purchased from BioLegend. All siRNAs used in CIA model were synthesized by Genepharma (Shanghai, China), and the sequences used were as follows: (i) IRF5: 5 -dTdT-CUG CAG AGA AUA ACC CUG A-dTdT-3 (sense) and 5 -dTdT UCA GGG UUA UUC UCU GCA G dTdT-3 (antisense). A dye was introduced to the 5′-end of the antisense strand of siIRF5. (ii) Negative control scrambled siRNA (siN.C).

### Human synovium specimens

Human synovial tissue sections were obtained from $ACPA^+$ RA patients ($n$ = 3) and healthy donors ($n$ = 3) of Department of orthopaedic surgery at Shandong Provincial Hospital Afliated to Shandong First Medical University. All samples were obtained with written informed consent and collected using a standard protocol approved under the Review Board protocol of Shandong First Medical University (Approval no. 2019-272).

**Cell culture**

Primary macrophages were derived from bone marrow-derived macrophages (BMDMs) of 7-8-week-old mice which were maintained in DMEM supplemented with 10% FBS and 1% penicillin/streptomycin. The femurs were dissected from the mouse. Then, the bone marrow was rinsed with 1× PBS to isolate bone marrow cells, which was followed by erythrocyte lysis in ACK lysis buffer. After centrifugation, the cells were resuspended in media with M-CSF (20 ng/ml) to induce the maturation of macrophages. After 72 hours of incubation, macrophage differentiation medium was discarded wash plates with sterile PBS to remove non-adherent cells. The adherent BMDMs were harvested and could be used in subsequent experiments for at least 7 days after induction. The BMDMs were collected after detachment with 0.05% trypsin EDTA and centrifugation at 400g for 5 min, and then the BMDMs were stained with PerCP-Cy5.5 conjugated anti-CD11b and FITC conjugated anti-F4/80 antibodies. The induction of mature macrophages was evaluated by flow cytometry (Beckman Coulter, USA).

Mouse neutrophils were collected from whole blood of C57BL/6 mice using the Percoll gradient method[35]. Briefly, before isolation of neutrophils, 1 mg/kg LPS was injected intraperitoneally into the mice to activate neutrophils in vivo. After 12 h, conduct the second injection. Three hours after the second injection, blood was collected by submandibular bleeding. Pooled blood was centrifuged (3,220g, 5 min, 4 ℃) and the buffy coat on top was added into a Percoll mixture solution consisting of 78%, 69% and 52% (v:v) Percoll in PBS, followed by centrifugation at 1500g for 30 min. The cell from the interface of the 69% and 78% gradient layers and the 78% fractions were recovered to a new tube. ACK lysis buffer was then added to the sample to lyse the erythrocytes. Neutrophils were purified by washing with ice-cold 1×PBS three times, and resuspend cells by culture medium (fig. S7).

**Synthesis of NBC-PtdSer**

The NBC-PtdSer was synthesized according to the procedure in Supplementary Scheme 1, 2. First, synthesis of NBC: 4-(Hydroxymethyl)phenylboronic acid pinacol

ester (0.25 g, 1.1 mmol) was dissolved in 10 ml of dry THF. Triethylamine (0.3 ml, 2.15 mmol) was added followed by 4-nitrophenyl chloroformate (0.27 g, 1.3 mmol) and the reaction was allowed to stir at room temperature for 12 h. The reaction was diluted with ethyl acetate and washed with 1.0 M HCl followed by saturated $NaHCO_3$. The organic layer was dried over $MgSO_4$, filtered and concentrated. NBC was purified on a silica gel column eluting with 5% EtOAc in hexanes to give 0.26 g (0.65 mmol, 61 % yield) as a white solid. The $^1H$ NMR spectrum of the product was obtained on a Bruker Advance DRX-400 spectrometer (Germany) with tetramethylsilane (TMS) as internal standard.

Then, synthesis of NBC-PtdSer: PtdSer (100 mg, 0.1344 mmol) and NBC (64.4 mg, 0.1613 mmol) were dissolved in dry DMF (3 ml) under an N atmosphere. After adding triethylamine (56 µl, 0.4032 mmol), the reaction was stirred 12 h before being quenched by pouring into 100 ml of 0.5 M HCl. The aqueous layer was extracted with 3 × 25 ml chloroform. The combined organic layer was washed with 5 × 100 ml water and once with brine. The collected organic phase was dried over $Na_2SO_4$, filtered, and concentrated under reduced pressure. The resulting crude was subjected to silica gel column chromatography. Gradient elution from 100% chloroform to 20% MeOH in chloroform was needed to purify the product as a white solid.

**Preparation and characterization of nano-formulation**

siIRF5@EINI were prepared using a modified water-in-oil reverse micro-emulsion protocol. Briefly, 500 µl of 30 mM $Zn(NO_3)_2 \cdot 6(H_2O)$ and 100 µl siIRF5 (siRNA at an input concentration of 200 nM) were dispersed in 20 ml cyclohexane/Igepal CO-520 (71/29V/V) solution to form a very well dispersed water-in-oil reverse micro-emulsion. To prepare the metformin loaded microemulsion, metformin solution (100 µl, 30 mM) and DOPA (100 µl, 35 mM) were added into a separate 20 ml oil phase. After mixing the above two microemulsions for 30 min to form the condensed cores, 40 ml of ethanol was added and the mixture was centrifuged at 12,500g for 20 min to remove cyclohexane and the surfactant. To prepared PtdSer-coroneted core, the pure pellets were suspended in 750 µl chloroform and mixed with 4 mg NBC-PtdSer. And then

evaporating the chloroform, 4 ml of 1× PBS was added to form PtdSer-coroneted core. Additionally, the corona of nanocore was cloaked with LWMH via a reversible boronate ester linker by the reaction of cis-diols and phenylboronic acid groups, and the efferocytosis-inspired nanoimitator was achieved.

The morphology and size of the nanoimitator was observed under a Hitachi H-7650 TEM (Hitachi, Japan) after negative staining with uranyl acetate solution (2%, wt/wt). The particle size distribution and zeta potential were measured by dynamic light scattering (DLS) using a Malvern Zetasizer Nano ZS. The PtdSer-presenting was validated by flow cytometry. Briefly, the nanoimitator was resuspended in PBS at pH 7.4 were incubated with or without $H_2O_2$ (0.1 mM). Then, these nano-formulations were incubated with FITC-Annexin V at the present of $Ca^{2+}$ for 15 min respectively and the binding rate of FITC-Annexin V was detected by flow cytometry. To quantify metformin release, the nanoimitator was resuspended in PBS at pH 5.0 or pH 7.4. At predetermined time points, aliquots from each group were centrifuged to pellet the nanoparticles, and the concentration of released metformin in the supernatant was measured using an HPLC system (Agilent 1100, USA) under the following chromatographic conditions: column, C18 column (5×250 mm, particle size 5 μm); mobile phase, methyl alcohol-15 mM $KH_2PO_4$ (60:40, v/v); flow rate, 1.0 ml/min; detection wavelength, 233 nm.

**Gel retardation assay**

Free siIRF5 and siIRF5@EINI (in 1×PBS) was separately mixed with loading buffer and loaded into 3% wt agarose gel with NA-Green (Beyotime Biotechnology Co., Ltd, China). Electrophoresis was conducted in 1×tris-acetate EDTA (TAE) buffer at 80 V for 30 min. To investigate the pH responsiveness, siIRF5@EINI was resuspended in PBS at pH 5.0 or pH 7.4 for 1 h. After that, the samples were analyzed by gel electrophoresis. The resulting gels were analysed using a UV illuminator (IS-2200; Alpha Innotech, San Leandro, CA, USA) to show the location of siIRF5.

**Macrophages targeting abilities of EINI in vitro**

BMDMs or FLSs were seeded in 6-well tissue culture plates at 50% confluency and cultured overnight. Cell culture medium was changed and 10 ng/ml recombinant human TNF-α was added to stimulate 4 h. The nanoimitator was then added into the cells with or without $H_2O_2$ (0.1 mM) pre-treating. After incubation, cells were washed three times with ice-cold PBS and fixed with 4% paraformaldehyde, then the cells were incubated at 37 °C for 10 min with 10 nM DAPI, and imaged with an EVOS inverted fluorescence microscope (Thermo Fisher Scientific). For flow cytometric analysis, cells were scraped and collected after PBS wash, then analysed with a Beckman Coulter Gallios flow cytometer. The results were analyzed using FlowJo software. To verify the specific macrophages homing of the nano-formulation, PKH67-labeled FLSs were cocultured with the unlabeled macrophages at a ratio of 1:1. Cells were stimulated with 10 ng/ml TNF-α for 4 h at 37 °C. $H_2O_2$ pretreated nanoimitator was added to the medium for 2 hours. The uptake of the nanoimitator was observed by CLSM.

**siRNA tracking and release in the cell**

To investigate endocytic pathways and intracellular release behavior of siIRF5, macrophages were treated with the siIRF5@EINI that were pre-conditioned with the 0.1mM of $H_2O_2$. At predetermined time, the treated cells were rinsed with PBS and incubated at 37 °C for 30 min with 100 nM LysoTracker Green in cell culture medium. After incubation, cells were washed with ice-cold PBS, fixed with 4% PFA 30 min at 4 °C, and followed by DAPI staining. The fluorescence imaging was performed by CLSM.

**Evaluation of the effects of nanoimitator on the adhesion and transmigration neutrophils**

For assaying the intervene effect on cell adhesion, $2\times10^5$ HUVECs were seeded in 6-well plate and pre-stimulated by incubation for 6 h with TNF-α (10 ng/ml). Then treated with RPMI medium, P-selectin antagonist (Human P-selectin/CD62P antibody, R&D Systems) and the nanoimitator for 30 min, respectively. $1\times10^6$ activated neutrophils were seeded on top of the treated endothelial monolayer. After 30 min at 37 °C under gentle shaking, each well was washed twice with PBS to remove the non-

adhered cells and labeled with FITC-labeled anti-Ly-6G antibody. Finally, evaluation of neutrophils adhered to HUVEC monolayers using CLSM and flow cytometry.

The inhibitory effects of the nanoimitator on the migration of neutrophils were evaluated by transwell assays. Prior to the experiment, the isolated neutrophils were pre-stimulated with 10 μM fMLF for 15 min at 37 ºC. The activated macrophages were treated with different formulations (the free siIRF5, 0.1 mM $H_2O_2$-pretreated siN.C@EINI and siIRF5@EINI) for 24 h. Cell media was collected and the bottom of transwell chambers was filled with cell media from each formulation. Then, $1\times10^6$ of preactivated neutrophils were seeded on 3 μm polycarbonate membrane. After incubation for 1 h, the neutrophils that migrated to the lower chamber were stained with crystal violet and counted. The results were expressed as a percentage of the total number of neutrophils added.

**Gene silencing assay**

IRF5 gene silencing efficiency of the nanoimitator was investigated by quantitative real-time PCR (qRT-PCR). Macrophages were seeded in a six-well plate ($1\times10^6$ cells per well) in growth medium for 24 hours. Cells were treated with TNF-α (10 ng/ml) for 6 h. The cells were incubated with the desired nano-formulations in 2 ml of fresh media. After 48 h, the cells were washed with PBS and the total RNA was extracted using the RNeasy Mini Kit (Qiagen) according to the manufacturer's instructions. Real-time quantitative PCR was performed to measure levels of mRNAs in macrophages encoding IRF5. β-actin was chosen as an internal housekeeping gene to normalize the IRF5 mRNA. The mRNA expression level was calculated based on comparative Ct method ($2^{-\triangle\triangle Ct}$). IRF5 blockade would have a major impact on reducing secretion level of macrophage-derived CXCL1, hence the CXCL1 mRNA expression was then evaluated by qRT-PCR. Real-time PCR was performed using specific primers (supplementary Table 1).

**Phenotype switching of macrophages**

For fluorescence immunostaining, macrophages were stimulated with TNF-α (10

ng/ml) to induce inflammation. Then, $H_2O_2$-pretreated nano-formulations were added to the media, and PBS and free siRNA were prepared in parallel for comparison. After 4 hours, the cells were incubated for another 24 hours. Cells were fixed with 4% PFA for 15 min and permeation with 0.1% Triton X 100 (room temperature, 10 min), the cells were blocked with normal rat serum (37 ºC, 1 h) and incubated with anti-iNOS or anti-CD206 antibody at 4 ºC overnight, followed by counterstaining with DAPI for 10 min. Fluorescence imaging was performed with confocal microscopy. qRT-PCR analysis was performed with the same procedure as mentioned above. The primer sequences were shown in supplementary Table 1.

**Collagen-induced arthritis (CIA) model and treatment protocols**

Autoimmune collagen-induced arthritic (CIA) mouse model was established by the following protocol. Immunization type II collagen (CII) lyophilized powder was dissolved in acetic acid (0.1 mol/l) and blended with an emulsion of complete Freund's adjuvant (CFA) in equal volume. Employed homogenizer to emulsify the mixture adequately in an ice bath. Next, healthy DBA/1 mice were intradermally injected the adjuvant (100 μl) at the tail root. The 2 times the dose immunization boost was given on day 21. The control group administrated solvent (acetic acid) injection.

To study therapeutic efficacy with CIA mice, the treatments began at day 7 after the second immunization. The CIA animals were randomly assigned into four groups (1 nmol of siRNA dose per mouse, 10 mg/kg metformin-equivalent dose, $n$ = 5). 200 μL PBS (G1); free siIRF5 solution (G2); siIN.C@EINI (G3) and siIRF5@EINI (G4) were administrated by tail vein twice a week from day 28 to 60.

**Study of the biodistribution of EINI in CIA model**

After boosting immunization for 7 days, DiR labeled nanoimitator was intravenously injected to CIA mice via tail vein. At predetermined time, the real-time imaging of nanoparticles in arthritis area was observed by the IVIS system (CRI, Inc., excitation: 748 nm, optical filter: 780 nm). At 48 h post injection, these mice were sacrificed to harvest the major organs (heart, liver, spleen, lung and kidneys) and inflamed paws, quantitatively assaying the clearance ratio of nanoformulations in vivo.

Specially, fluorescence molecular tomography computed tomography (FMT-CT) on day 2 postinjection to identify nanoimitator localization in the inflamed regions. For observation of the specific homing of the nanoimitator to inflamed synovium, 100 μl of Cy5.5 labeled nano-formulation were injected into CIA mice via the tail vein, with free Cy5.5 labeled siIRF5 as a control. After 72 h, the mice were euthanized, and the synovium was obtained and fixed with 4% PFA 48 h at 4 ºC. After dehydration and embedded in Tissue-Tek OCT Compound (Sakura Finetek) for frozen sectioning. And then the slides were stained with anti-F4/80 antibodies, followed by DAPI staining. The fluorescence imaging was performed by CLSM.

**qRT-PCR analysis of IRF5 expressions from collected synovial macrophages**

Fresh synovial tissues were digested with 1 mg/ml type I collagenase in HBSS, and incubated at 37 ºC, 5% $CO_2$ in a humidified atmosphere for 30-45 min. Disaggregated tissue elements were passed through a 70 μm cell strainer. Synovial macrophages (CD45+, CD11b+, F4/80$^{high}$, Ly6G-, Ly6C$^{Low}$)[36] were sorted on a BECKMAN Moflo Astrios EQ (BECKMAN Coulter). Next, total RNA was isolated by following manufacturer instructions. Synthesis of cDNA and qRT-PCR was performed as previously described in vitro analysis.

**Histological analysis of inflamed joints**

Histopathology was evaluated to determine the features of RA including neutrophils migration, macrophage phenotype, angiogenesis, synovitis, and cartilage destruction. At study endpoints, mice were euthanized and hind ankle joints were collected for H&E staining, safranin-O or TRAP staining. To detect infiltration of neutrophils, joint sections were dewaxed, and stained with primary antibodies anti-MPO (Bioss Antibodies). Biotinylated anti-rabbit IgG was used as the secondary antibody for chromagen development. For evaluation of phenotype switching of macrophages, tissue sections were stained with antibodies anti-iNOS or anti-CD206. Tissue sections were then stained with DAPI mounting solution, and observed using CLSM.

Dissected the hind paw joints were evaluated with micro-computed tomography

(micro-CT) imaging. Micro-CT scanning parameters were voxel size, 9 μm; voltage, 90 kV; current, 88 μA; exposure time, 4 min. To compare the therapeutic effect in each group, three-dimensional images were reconstructed using Mimics software (Materialise) and the mean bone mineral density (BMD) of the joints, were calculated by software CTAn (Skyscan).

**Histological scoring of mouse arthritic joints**

Histopathological scoring was performed as described grading scheme[37]. Briefly, joints of arthritic mice were assigned scores of 0 to 4 for inflammation based on H&E staining, according to the following criteria: 0 = normal; 1 = minimal infiltration of inflammatory cells in periarticular area; 2 = mild infiltration; 3 = moderate infiltration; and 4 = marked infiltration. Cartilage depletion was identified by diminished Safranin O staining of the matrix and was scored on a scale of 0 to 4, where 0 = no cartilage destruction (full staining with Safranin O), 1 = localized cartilage erosions, 2 = more extended cartilage erosions, 3 = severe cartilage erosions, and 4 = depletion of entire cartilage. Histologic evaluations were performed in a blinded manner.

**Statistical analysis**

Results are presented as mean ± s.d. Error bars represent the s.d. of the mean from independent samples. Two-tailed Student's t-test was applied to test the statistical significance of difference between two groups. For multiple comparisons, the data were analyzed using a one-way analysis of variance (ANOVA). All statistical analyses were carried out with Prism software package (PRISM 8.3.0; GraphPad Software). Statistical significance was set at $*P < 0.05$, $**P < 0.01$, $***P < 0.001$, $****P < 0.0001$.

**Data and materials availability:** The data that support the plots within the paper and other findings of this study are available from the corresponding author upon reasonable request. IRF5 mRNA expression level in patients with RA retrieved from the ArrayExpress (https://www.ebi.ac.uk/arrayexpress/) under Accession code E-MTAB-6141[38].

## References


1. Sparks JA. Rheumatoid Arthritis. *Annals of Internal Medicine* **170**, ITC1-ITC16 (2019).
2. Firestein GS, McInnes IB. Immunopathogenesis of Rheumatoid Arthritis. *Immunity* **46**, 183-196 (2017).
3. Guo Q, Wang Y, Xu D, Nossent J, Pavlos NJ, Xu J. Rheumatoid arthritis: pathological mechanisms and modern pharmacologic therapies. *Bone Research* **6**, 15 (2018).
4. Feldmann M, Maini RN. Perspectives From Masters in Rheumatology and Autoimmunity: Can We Get Closer to a Cure for Rheumatoid Arthritis? *Arthritis & Rheumatology* **67**, 2283-2291 (2015).
5. Richter A*, et al.* Impact of treatment with biologic DMARDs on the risk of sepsis or mortality after serious infection in patients with rheumatoid arthritis. *Annals of the Rheumatic Diseases* **75**, 1667-1673 (2016).
6. McInnes IB, Schett G. Cytokines in the pathogenesis of rheumatoid arthritis. *Nature Reviews Immunology* **7**, 429-442 (2007).
7. Smolen JS*, et al.* Rheumatoid arthritis. *Nature Reviews Disease Primers* **4**, 18001 (2018).
8. Udalova IA, Mantovani A, Feldmann M. Macrophage heterogeneity in the context of rheumatoid arthritis. *Nature Reviews Rheumatology* **12**, 472-485 (2016).
9. Di Benedetto P, Ruscitti P, Vadasz Z, Toubi E, Giacomelli R. Macrophages with regulatory functions, a possible new therapeutic perspective in autoimmune diseases. *Autoimmunity Reviews* **18**, 102369 (2019).
10. Matthijssen XME, Niemantsverdriet E, Huizinga TWJ, van der Helm–van Mil AHM. Enhanced treatment strategies and distinct disease outcomes among autoantibody-positive and -negative rheumatoid arthritis patients over 25 years: A longitudinal cohort study in the Netherlands. *PLOS Medicine* **17**, e1003296 (2020).
11. Malmström V, Catrina AI, Klareskog L. The immunopathogenesis of seropositive rheumatoid arthritis: from triggering to targeting. *Nature Reviews Immunology* **17**, 60-75 (2017).
12. Krausgruber T*, et al.* IRF5 promotes inflammatory macrophage polarization and TH1-TH17 responses. *Nature Immunology* **12**, 231-238 (2011).
13. Takaoka A*, et al.* Integral role of IRF-5 in the gene induction programme activated by Toll-like receptors. *Nature* **434**, 243-249 (2005).
14. Weiss M*, et al.* IRF5 controls both acute and chronic inflammation. *Proceedings of the National Academy of Sciences* **112**, 11001-11006 (2015).
15. Dieguez-Gonzalez R*, et al.* Association of interferon regulatory factor 5 haplotypes, similar to that found in systemic lupus erythematosus, in a large subgroup of patients with rheumatoid arthritis. *Arthritis & Rheumatism* **58**, 1264-1274 (2008).
16. Graham RR*, et al.* A common haplotype of interferon regulatory factor 5 (IRF5) regulates splicing and expression and is associated with increased risk of

systemic lupus erythematosus. *Nature Genetics* **38**, 550-555 (2006).
17. Henson PM. Cell Removal: Efferocytosis. *Annual Review of Cell and Developmental Biology* **33**, 127-144 (2017).
18. Poon IKH, Lucas CD, Rossi AG, Ravichandran KS. Apoptotic cell clearance: basic biology and therapeutic potential. *Nature Reviews Immunology* **14**, 166-180 (2014).
19. Segawa K, Nagata S. An Apoptotic 'Eat Me' Signal: Phosphatidylserine Exposure. *Trends in Cell Biology* **25**, 639-650 (2015).
20. Fearon U, Canavan M, Biniecka M, Veale DJ. Hypoxia, mitochondrial dysfunction and synovial invasiveness in rheumatoid arthritis. *Nature Reviews Rheumatology* **12**, 385-397 (2016).
21. Phull A-R, Nasir B, Haq Iu, Kim SJ. Oxidative stress, consequences and ROS mediated cellular signaling in rheumatoid arthritis. *Chemico-Biological Interactions* **281**, 121-136 (2018).
22. Wang L, Brown JR, Varki A, Esko JD. Heparin's anti-inflammatory effects require glucosamine 6-O-sulfation and are mediated by blockade of L- and P-selectins. *The Journal of Clinical Investigation* **110**, 127-136 (2002).
23. Liddiard K, Taylor PR. Understanding Local Macrophage Phenotypes In Disease: Shape-shifting macrophages. *Nature Medicine* **21**, 119-120 (2015).
24. Mills EL, O'Neill LA. Reprogramming mitochondrial metabolism in macrophages as an anti-inflammatory signal. *European Journal of Immunology* **46**, 13-21 (2016).
25. Soberanes S*, et al.* Metformin Targets Mitochondrial Electron Transport to Reduce Air-Pollution-Induced Thrombosis. *Cell Metabolism* **29**, 335-347 (2019).
26. Brand DD, Latham KA, Rosloniec EF. Collagen-induced arthritis. *Nature Protocols* **2**, 1269-1275 (2007).
27. Meehan GR*, et al.* Preclinical models of arthritis for studying immunotherapy and immune tolerance. *Annals of the Rheumatic Diseases*, annrheumdis-2021-220043 (2021).
28. Cecchi I*, et al.* Neutrophils: Novel key players in Rheumatoid Arthritis. Current and future therapeutic targets. *Autoimmunity Reviews* **17**, 1138-1149 (2018).
29. Lainer-Carr D, Brahn E. Angiogenesis inhibition as a therapeutic approach for inflammatory synovitis. *Nature Clinical Practice Rheumatology* **3**, 434-442 (2007).
30. Zhang F*, et al.* Defining inflammatory cell states in rheumatoid arthritis joint synovial tissues by integrating single-cell transcriptomics and mass cytometry. *Nature Immunology* **20**, 928-942 (2019).
31. Boutet M-A*, et al.* Novel insights into macrophage diversity in rheumatoid arthritis synovium. *Autoimmunity Reviews* **20**, 102758 (2021).
32. Safiri S*, et al.* Global, regional and national burden of rheumatoid arthritis 1990–2017: a systematic analysis of the Global Burden of Disease study 2017. *Annals of the Rheumatic Diseases* **78**, 1463-1471 (2019).
33. Tietjen GT*, et al.* Molecular mechanism for differential recognition of

membrane phosphatidylserine by the immune regulatory receptor Tim4. *Proceedings of the National Academy of Sciences* **111**, E1463-E1472 (2014).
34. Ryan DG, O'Neill LAJ. Krebs Cycle Reborn in Macrophage Immunometabolism. *Annual Review of Immunology* **38**, 289-313 (2020).
35. Zhang Q*, et al.* Neutrophil membrane-coated nanoparticles inhibit synovial inflammation and alleviate joint damage in inflammatory arthritis. *Nature Nanotechnology* **13**, 1182-1190 (2018).
36. Ammari M*, et al.* Delivery of miR-146a to Ly6C<sup>high</sup> Monocytes Inhibits Pathogenic Bone Erosion in Inflammatory Arthritis. *Theranostics* **8**, 5972-5985 (2018).
37. Doody Karen, M. et al. Targeting phosphatase-dependent proteoglycan switch for rheumatoid arthritis therapy. *Science Translational Medicine* **7**, 288ra276 (2015).
38. Lewis, M.J. et al. Molecular Portraits of Early Rheumatoid Arthritis Identify Clinical and Treatment Response Phenotypes. *Cell Reports* **28**, 2455-2470. (2019).

**Acknowledgments:** This work was supported by National Natural Science Foundation of China (82173763), Shandong Provincial Key Research and Development Program (Major Scientific and Technological Innovation Project) (2021CXGC010515), Funds for Youth Interdisciplinary and Innovation Research Groups of Shandong University (2020QNQT003), Major New Drug Creation Project of China (2017ZX09301064). Thanks for the technical support from Y. Yu, X.-M. Yu, J. Zhang, M.-L. Wu and L.-M. Wang in Advanced Medical Research Institute/Translational Medicine Core Facility of Advanced Medical Research Institute, Shandong University.

**Author contributions:** X.J. and S.Z. conceived the study and designed experiments. S.Z. and Q.C. characterized properties of the materials. S.Z., Q.C., C.T. and Z.L. performed the animal experiments. Z.M., C.C., J.Z., Y.L. P.S., R.Z., Z.Y., Y.W. and M.H. contributed to data analysis and interpretation. S.Z. crafted all the figures and wrote the manuscript. X.J., M.M., W.L., X.W., G.Y., B.S., and J.L. edited and revised the manuscript and supervised the research.

**Competing interests:** The authors declare that they have no competing interests.

**Supplementary Information for**

# Remodeling Articular Immune Homeostasis with an Efferocytosis-inspired Nanoimitator Mitigates Rheumatoid Arthritis

Shengchang Zhang[1], Qihao Chai[2,3], Chunwei Tang[1], Ziyang Li[2,3], Zhentao Man[2,3], Chen Chen[1], Jing Zhang[1], Ying Liu[1], Peng Sun[4], Rui Zhang[1], Zhenmei Yang[1], Maosen Han[1], Yan Wang[1], Xia Wei[5], Jun Li[5], Wei Li[2,3], Mohnad Abdalla[1], Gongchang Yu[6], Bin Shi[6], Xinyi Jiang[1,7*]

[*]Corresponding author: Xinyi Jiang, Ph.D.

Phone/Fax：+86-15662758621

Email：xinyijiang@sdu.edu.cn

**Contents**

**Supplementary Scheme 1. Synthetic of NBC.**

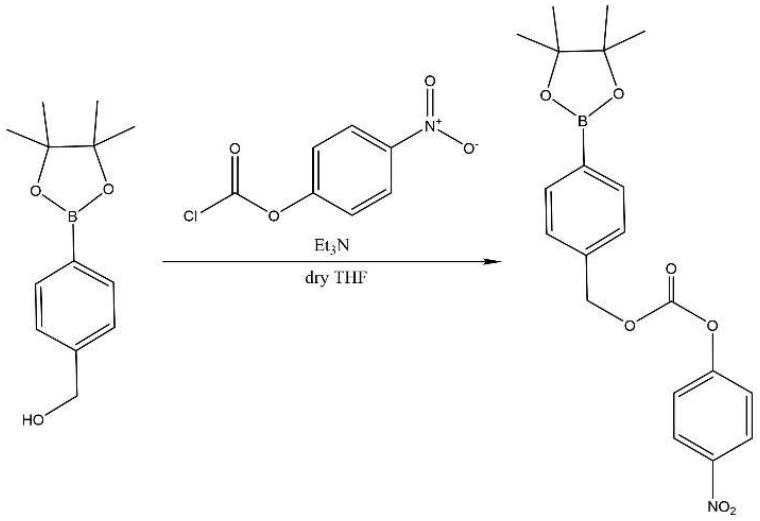


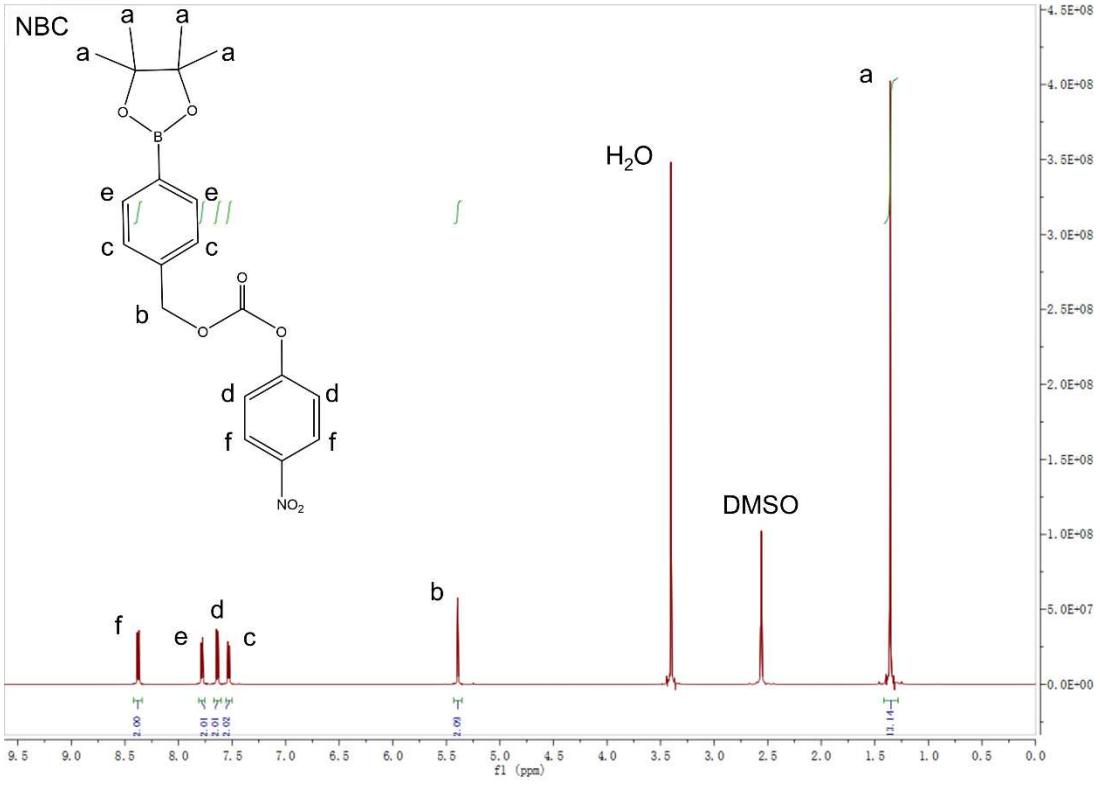


**Supplementary Figure 1. $^{1}$H NMR spectrum of NBC in DMSO-d6.**

**Supplementary Scheme 2. Synthetic route developed to produce PtdSer-NBC.**

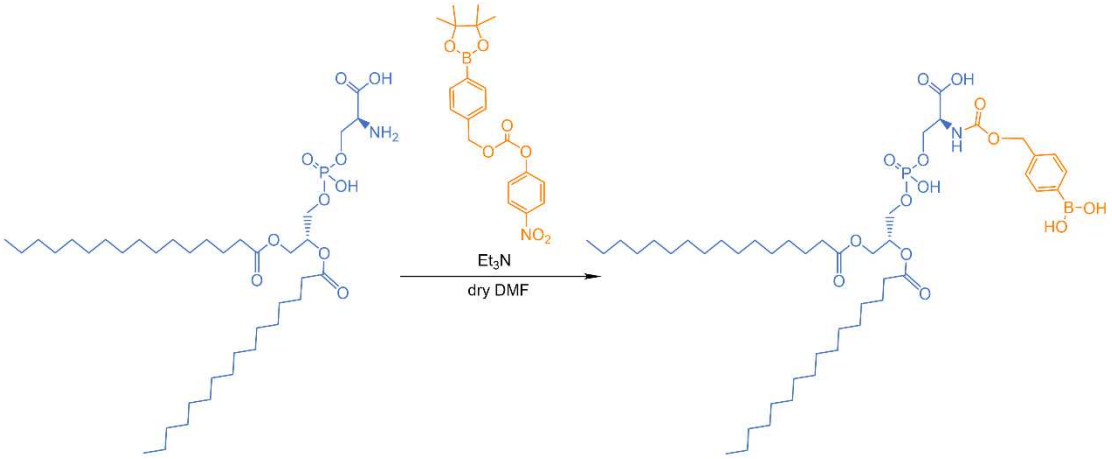


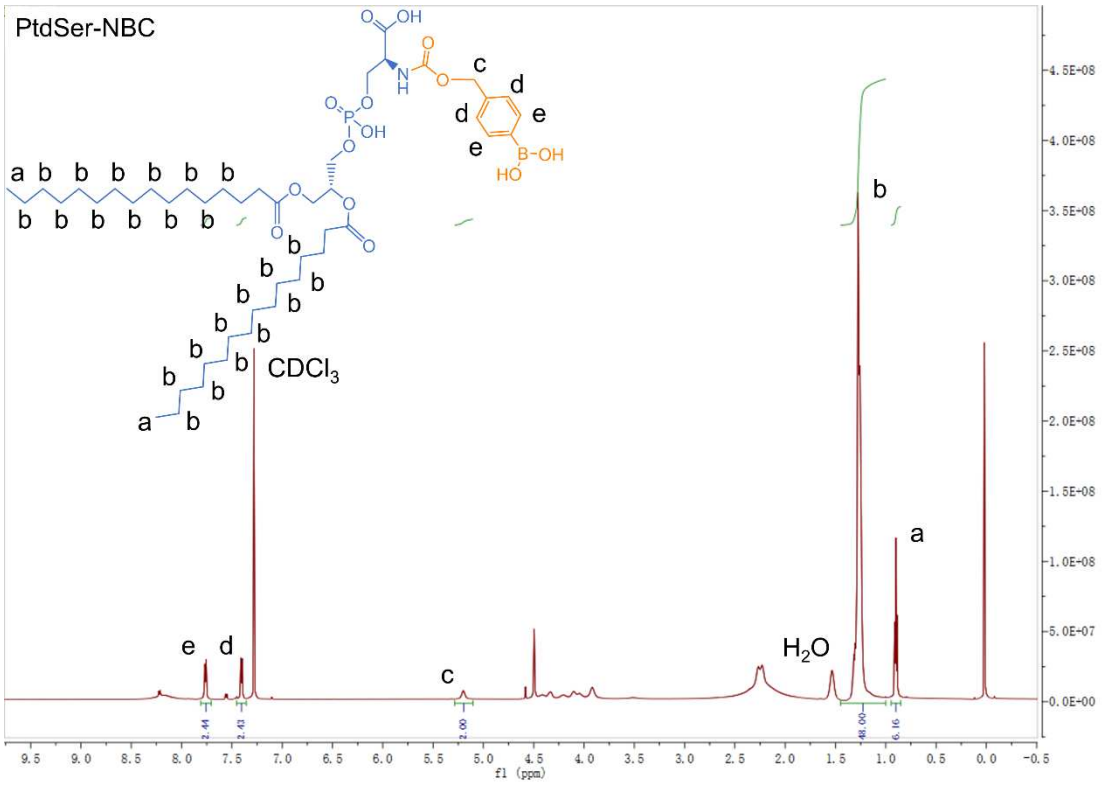


**Supplementary Figure 2. $^{1}$H NMR spectrum of PtdSer-NBC in $CDCl_3$.**

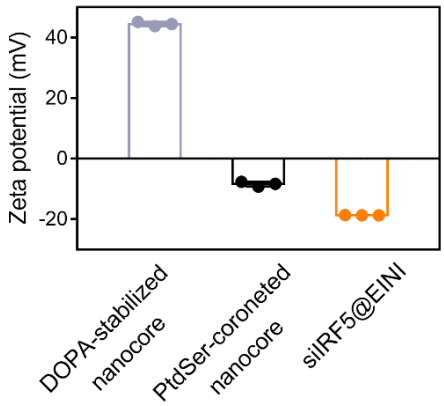


**Supplementary Figure 3. Zeta potential of DOPA-stabilized nanocore, PtdSer-coroneted nanocore and siIRF5@EINI.**

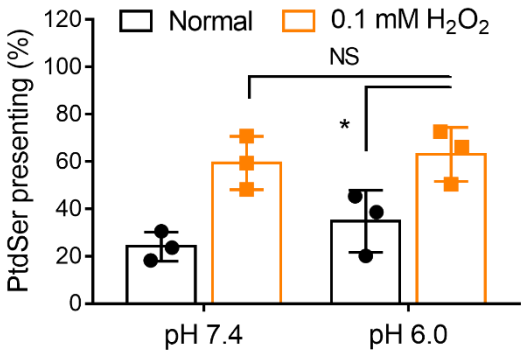


**Supplementary Figure 4. Flow cytometry analysis of PtdSer-presenting.** The nanoimitator was resuspended in PBS at pH 7.4 or pH 6.0 respectively, and was incubated with or without $H_2O_2$ (0.1 mM). Data are presented as the mean ± s.d. ($n = 3$ independent experiments). $^{**}P < 0.01$. NS, not significant.

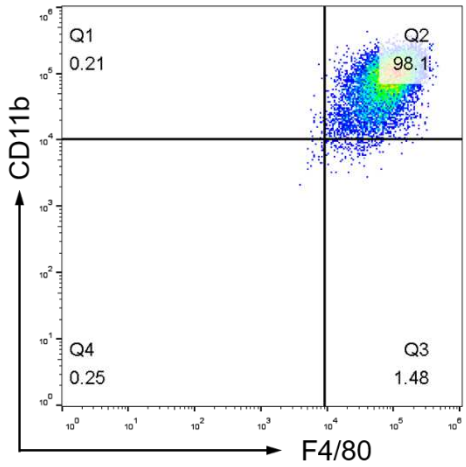


**Supplementary Figure 5. The expression levels of CD11b and F4/80 in BMDMs analyzed by flow cytometry.**

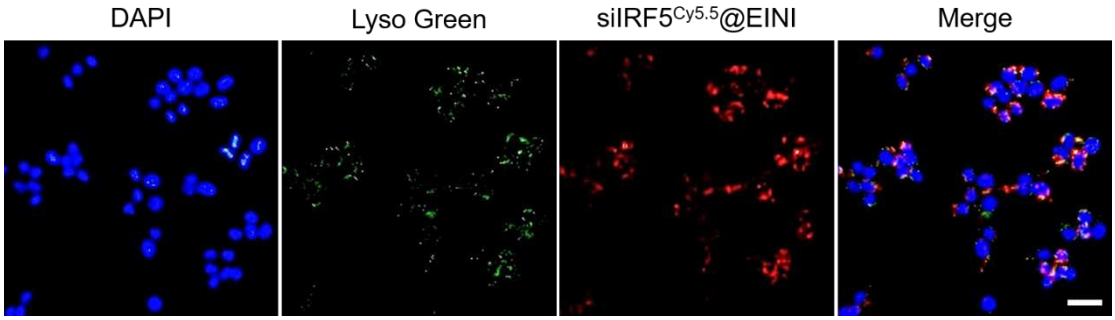


**Supplementary Figure 6. Fluorescent visualization of siRNA localization in macrophages 6 hours after incubation with nanoimitator. Scale bars, 50 nm.**

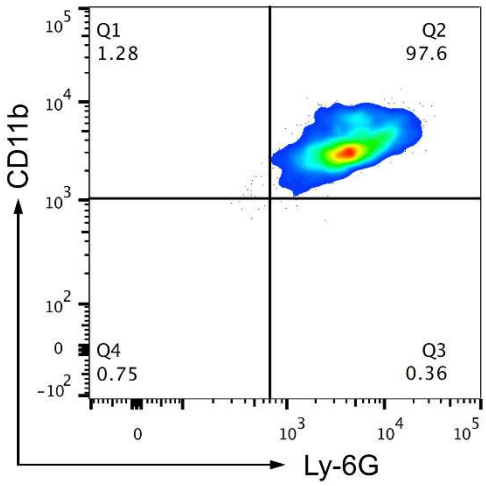


**Supplementary Figure 7. Flow cytometric analysis of the purity of neutrophils doubly stained with FITC-conjugated Ly-6G and PerCP-Cy5.5-conjugated CD11b antibodies.**

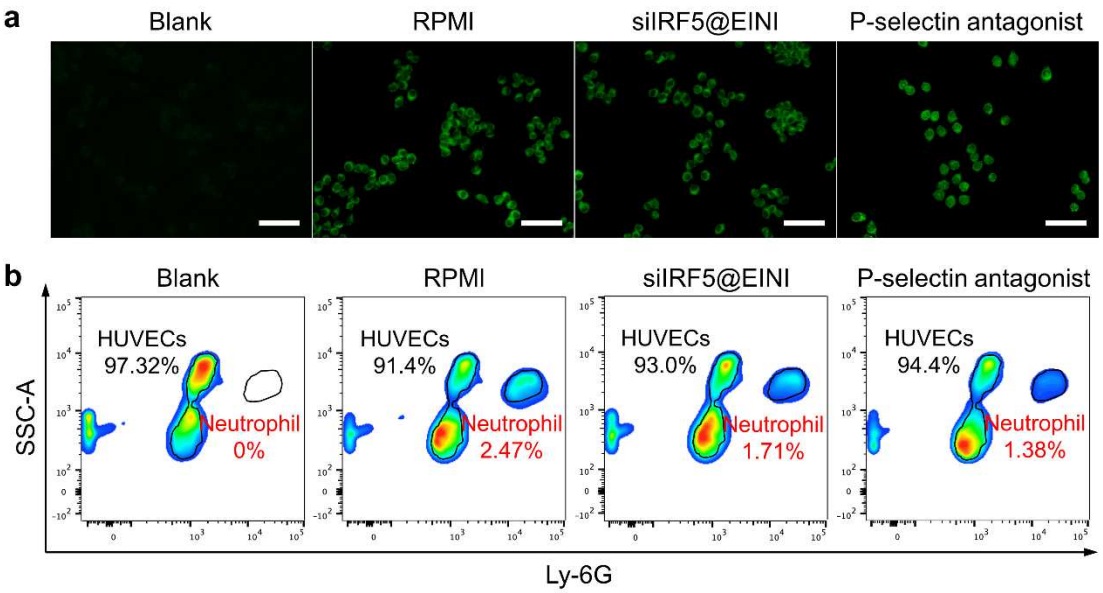


**Supplementary Figure 8. Effective intervention by nanoimitator on inflammatory neutrophils. a**, Evaluation of neutrophil adhesion to a HUVECs monolayer after incubation with nanoimitator. Scale bars, 50 nm. **b**, FACS analysis of neutrophil adhesion to HUVECs. All values are expressed as the mean ± s.d. ($n$ = 3 independent experiments).

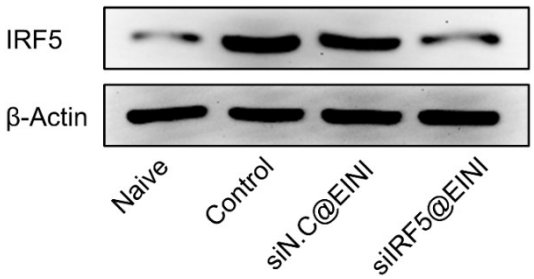


**Supplementary Figure 9. IRF5 expression in macrophages treated with different formulations, detected by western blot.**

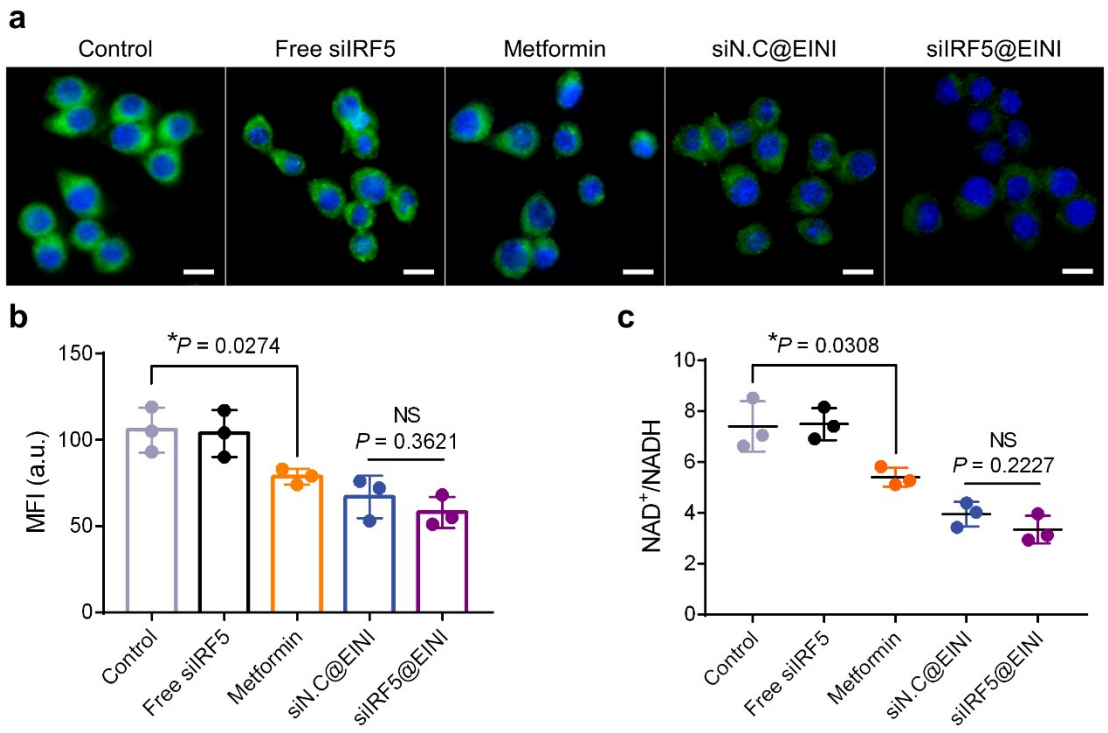


**Supplementary Figure 10. Metformin reprogramming mitochondrial metabolism in macrophages, which act as mitochondrial complex I (CI) inhibitor directly inhibit CI-derived ROS. a**, Fluorescence images and the quantification result (**b**) of intracellular ROS generation in macrophages stained with DCFH-DA. The scale bars were 20 μm. **c**, The levels of oxidized and reduced nicotinamide adenine dinucleotide ($NAD^+$/NADH) were measured in macrophages using a colorimetric assay. All values are expressed as the mean ± s.d. ($n$ = 3 biologically independent animals). *$P$ < 0.05. NS, not significant.

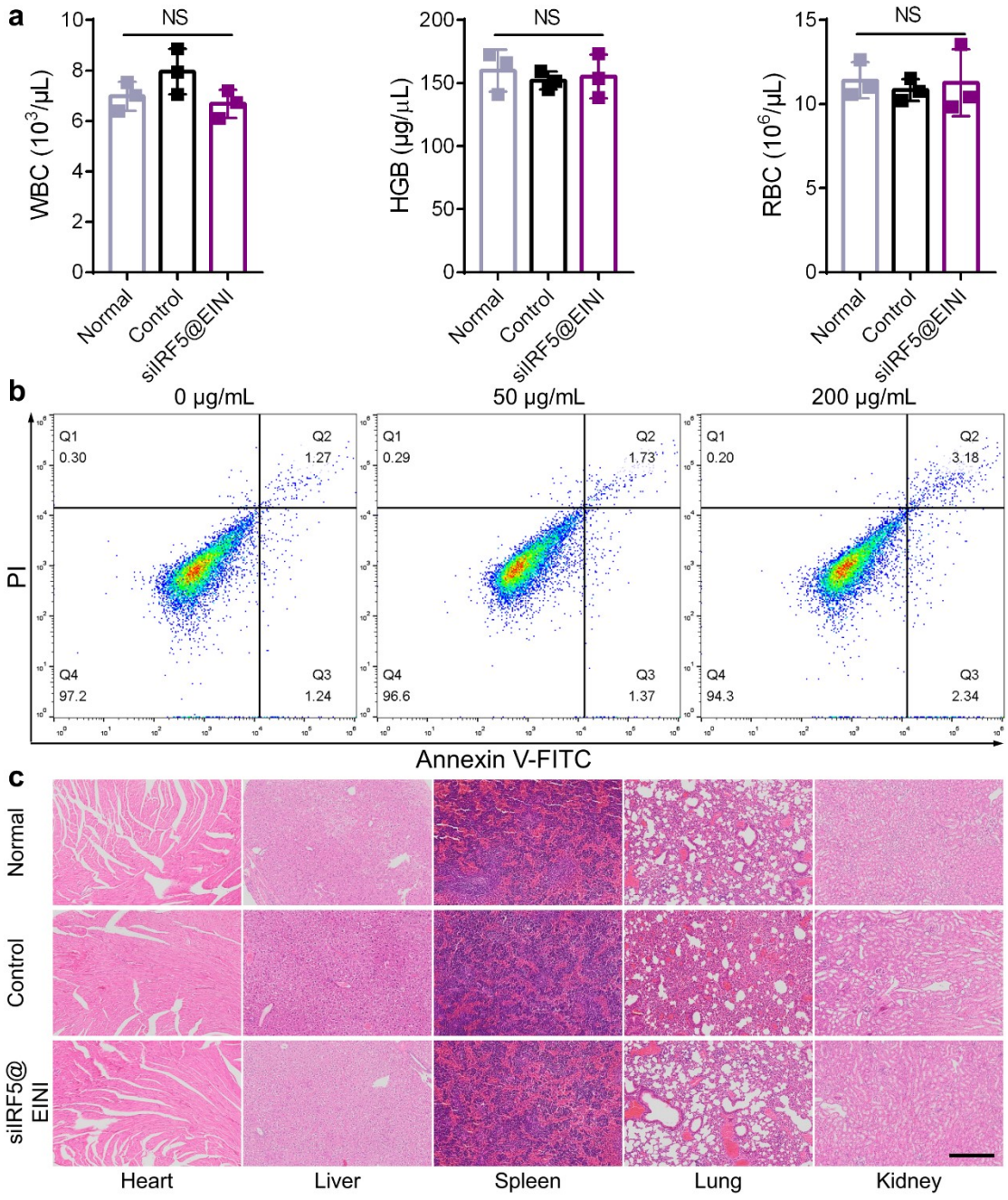


**Supplementary Figure 11. Systemic toxicity evaluation of siIRF5@EINI. a**, During the experimental cycle, mice were followed up to sacrifice on day 60, the change of white blood cell (WBC), hemoglobin (HGB) and red blood cell (RBC) were measured. Data are presented as the mean ± s.d. ($n$ = 3 independent experiments). NS, not significant. **b**, Apoptosis of T cells extracted from the spleens of mice that received i.v. injections of siIRF5@EINI during the experimental cycle. Mice injected with PBS were used as a negative control. **c**, Histological sections of major organs at 60th day. Scale bar, 50 μm. ($n$ = 3 biologically independent animals).

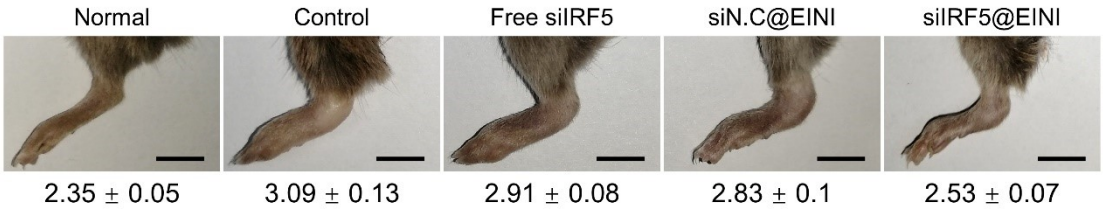


**Supplementary Figure 12. Representative lesions image from macroscopic observation of the hind paws in different treatment groups. Scale bar, 3 mm. (*n* = 5 biologically independent animals).**

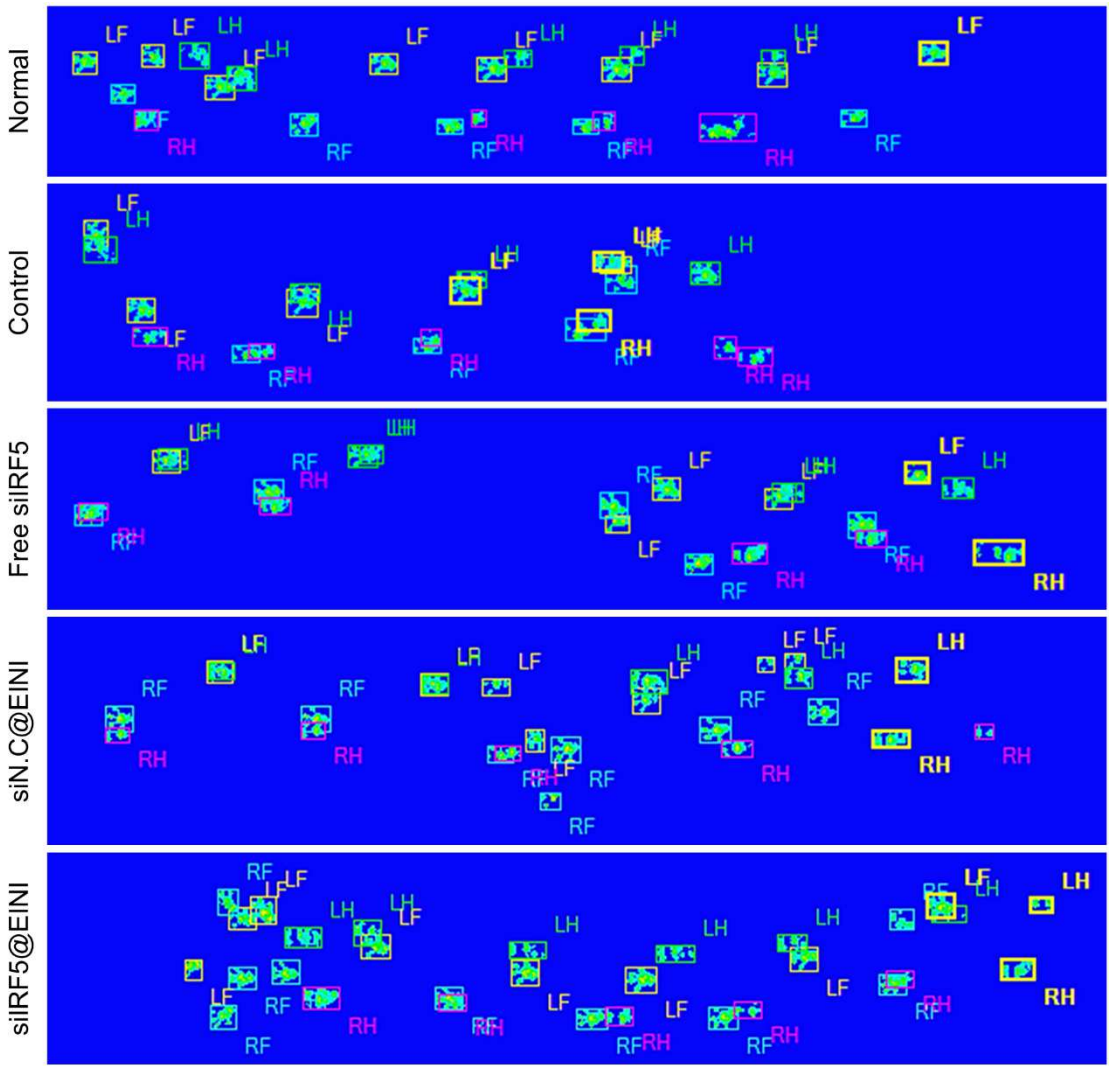


**Supplementary Figure 13. Representative signal images of the footprint assay.**

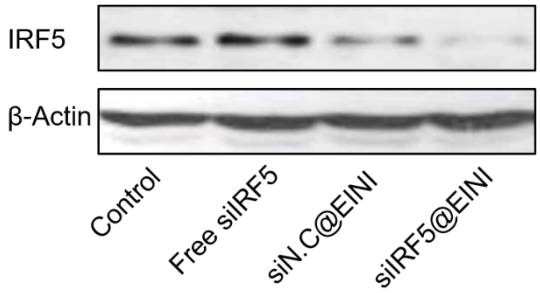


**Supplementary Figure 14. Western blot images of IRF5 protein levels in the synovial macrophages in different formulations treated group.**

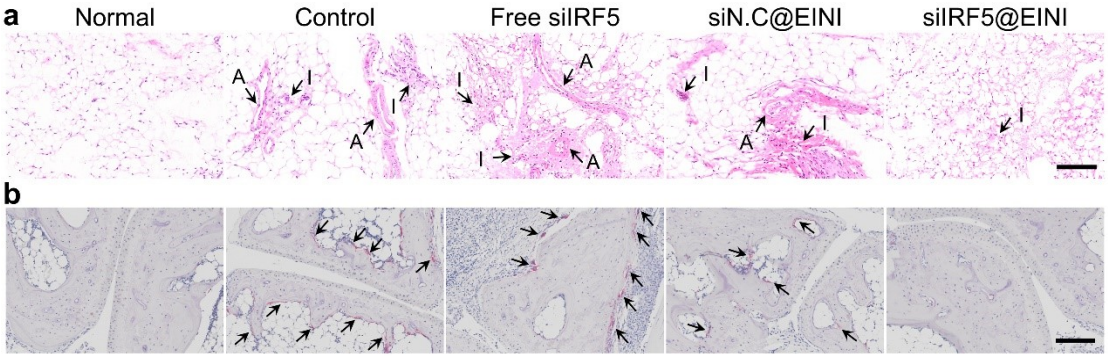


**Supplementary Figure 15. H&E staining of synovium and immunohistochemical analyses of the TRAP-stained osteoclasts. a**, H&E staining of synovium extracted from mice of different treatment groups. I, immune cell infiltration; A, angiogenesis. Scale bars = 50 μm. (*n* = 5 biologically independent animals). **b**, Immunohistochemical analyses of the TRAP-stained osteoclasts in the joint tissues from rats receiving the indicated treatment. Scale bar = 100 μm. (*n* = 5 biologically independent animals).

Supplementary Table 1. List of primers used for real-time PCR

| | | |
|---|---|---|
| IRF5 | Forward | 5’-CATTCAGCGGGAAGTCAAGA-3’ |
| | Reverse | 5’-TGTCTGCCGACCAAGAAAGC-3’ |
| CXCL1 | Forward | 5’-CACCCAAACCGAAGTCATAGC-3’ |
| | Reverse | 5’-GGGGACACCTTTTAGCATCTTT-3’ |
| iNOS | Forward | 5'-AGCCAAGCCCTCACCTACTT-3’ |
| | Reverse | 5'-CTCTGCCTATCCGTCTCGTC-3’ |
| TNF-α | Forward | 5’-TGGAACTGGCAGAAGAGGCAC-3’ |
| | Reverse | 5’-AGGGTCTGGGCCATAGAACTGA-3’ |
| Arg1 | Forward | 5’-TGCTTAGCTCTGTCTGCTTTGC-3’ |
| | Reverse | 5’-GAACACGGCAGTGGCTTTAAC-3’ |
| CD206 | Forward | 5’-GGAGGCTGATTACGAGCAGT-3’ |
| | Reverse | 5’-CATAGGAAACGGGAGAACCA-3’ |
| β-actin | Forward | 5'-CTACAATGAGCTGCGTGTGG-3’ |
| | Reverse | 5'-CAGGTCCAGACGCAGGATGGC-3’ |

# Supplementary Files

This is a list of supplementary files associated with this preprint. Click to download.

- SupplementaryInformation.pdf